IMMUNOLOGY

Conserved noncoding sequence-9 regulates NFATc1-mediated IL-10 expression in B cells to control inflammatory responses

Seung Won Kim[1], Jaegyun Noh[1], Hye Eun Park[1], Ki Hurn So[1], Won Hwang[1]†, Gi-Chen Kim‡, Chan Johng Kim[1]§, Jae-Seon So[2]*, Sin-Hyeog Im[1,3,4]*

Interleukin-10 (IL-10) production by B cells plays a critical role in regulating inflammatory responses, yet the mechanisms controlling its expression remain poorly understood. We identified a conserved noncoding sequence (CNS-9) as an essential regulatory element for IL-10 expression in mouse B cells. Comprehensive genomic analyses revealed that CNS-9 functions as an enhancer bound by the transcription factor NFATc1, which facilitates chromatin looping between CNS-9 and the IL-10 promoter to drive transcription. Flow cytometry analyses identified B1a cells as the predominant source of B cell-derived IL-10, with this production critically dependent on NFATc1-mediated CNS-9 regulation. In a mouse model of LPS-induced sepsis, deletion of CNS-9, B cell–specific NFATc1, or both resulted in reduced IL-10 production, exacerbated inflammatory responses, and decreased survival. Furthermore, we demonstrated that the human homolog, CNS-12, functions similarly through NFATc1-dependent mechanisms. These findings establish a conserved regulatory pathway controlling IL-10 expression in B cells with notable implications for inflammatory disease pathogenesis and potential therapeutic interventions.

INTRODUCTION

Interleukin-10 (IL-10) is an anti-inflammatory cytokine that plays a crucial role in maintaining immune homeostasis (*1*, *2*). It primarily functions by limiting excessive inflammatory responses and preventing tissue damage during autoimmunity and infections. Mice deficient in IL-10 spontaneously develop inflammatory bowel disease and exhibit heightened susceptibility to septic shock when exposed to low doses of lipopolysaccharide (LPS), indicating an immunomodulatory function of IL-10 (*3*, *4*).

IL-10 can be produced by various types of immune cells, including macrophages, dendritic cells, T cells, and B cells (*5*). However, B cells are the predominant cellular source of IL-10 in the lymphoid tissues of both naive and endotoxemia-challenged mice, suggesting their essential role in immune regulation (*6*). B cell–derived IL-10 exerts diverse immunomodulatory functions by suppressing pathogenic T cell responses, down-regulating the activation of dendritic cells and macrophages, and limiting the production of pro-inflammatory cytokines by myeloid cells (*7*–*9*). Among B cell subsets, B1a cells, in particular, have been identified as major IL-10 producers (*10*). Studies have demonstrated that IL-10 deficiency in B1a cells exacerbates disease severity in experimental models of autoimmunity, infection, and sepsis (*11*, *12*). Despite the established importance of B cell–derived IL-10 in immune homeostasis, the molecular mechanisms governing its expression remain poorly understood.

The transcriptional regulation of genes involves complex interactions between promoters and cis-regulatory elements, predominantly enhancers and silencers. Most of these regulatory elements are characterized as conserved noncoding sequences (CNSs) (*13*). These CNSs can be identified through their evolutionary conservation, chromatin accessibility, and distinctive epigenetic signatures, including the enrichment of enhancer-associated histone modifications (H3K4me1, H3K27ac) and coactivators, such as p300 (*14*–*19*).

Several studies have provided important insights into the regulation of IL-10 expression in various immune cell populations, including T cells, dendritic cells, and macrophages (*20*–*22*). Previously, we identified a distal cis-acting element, known as CNS-9, which exhibits robust enhancer activity in T helper 2 (T_H2) cells (*23*). In that study, NFATc2 and IRF4 are selectively recruited to the CNS-9 region and synergistically enhance its function. In macrophages, LPS-induced *Il10* transcription is regulated by RelA binding to another regulatory region, CNS-4.5 (*24*). However, *Il10* gene regulation in B cells is still poorly characterized.

B cell receptor (BCR) engagement is fundamental for B cell development, differentiation, survival, and immune responses as it activates multiple transcription factors, including members of the nuclear factor of activated T cells (NFAT) family and nuclear factor κB (NF-κB) (*25*–*27*). NFAT proteins comprise a family of calcium-dependent transcription factors, including NFATc1, NFATc2, NFATc3, and NFATc4, which play essential roles in immune cell function (*28*). The activation of NFAT proteins involves their dephosphorylation by the calcium-dependent phosphatase calcineurin, which facilitates their nuclear translocation and subsequent binding to the promoters and enhancers of target genes (*29*). The pharmacological inhibition of calcineurin activity by cyclosporine A (CsA) or FK506 prevents the nuclear translocation of NFAT proteins (*30*). While NFAT proteins are known to regulate the expression of various cytokines, including IL-2, IL-4, and IL-10 in T cells, their role in cytokine production in B cells, particularly IL-10, remains incompletely defined.

In this study, we aimed to identify the key regulatory elements and transcription factors controlling *Il10* expression in B cells. Through an

[1]Department of Life Sciences, POSTECH Biotech Center, Pohang University of Science and Technology (POSTECH), Pohang 37673, Republic of Korea. [2]Department of Biopharmaceutical Engineering, Dongguk University WISE, Gyeongju 38066, Republic of Korea. [3]ImmmunoBiome Inc., 77 Cheongam-Ro, Nam-Gu, Pohang 37673, Republic of Korea. [4]Institute for Convergence Research and Education, Yonsei University, Seoul 03722, Republic of Korea.
*Corresponding author. Email: sojs@dongguk.ac.kr (J.-S.S.); iimsh@postech.ac.kr (S.-H.I.)
†Present address: MSBIOTECH CO., LTD R&D Center, 25 Misan-gil, Daeso-myeon, Eumseong-gun, Chungcheongbuk-do 27672, Republic of Korea.
‡Present address: Department of Microbiology and Immunology, Yonsei University College of Medicine, Seoul 03722, Republic of Korea.
§Present address: Department of Biochemistry and Institute for Protein Design, University of Washington, Seattle, WA 98195, USA.

integrated genomic approach combining assay for transposase-accessible chromatin sequencing (ATAC-seq), RNA sequencing (RNA-seq), and chromatin immunoprecipitation sequencing (ChIP-seq) analyses, we identified CNS-9 as a key enhancer element for *Il10* expression in B cells. We demonstrated that NFATc1 specifically binds to CNS-9 and mediates chromatin looping between this enhancer and the *Il10* promoter, thereby driving *Il10* transcription. Furthermore, the genetic deletion of either CNS-9 or B cell–specific NFATc1 impaired IL-10 production and exacerbated inflammatory responses in the LPS-induced sepsis model. Last, we identified and functionally characterized the human homolog of murine CNS-9, designated as CNS-12, revealing a conserved regulatory mechanism for *IL10* expression in human B cells. These findings provide insights into the molecular mechanisms governing B cell–derived IL-10 production and highlight potential therapeutic targets for modulating IL-10 expression in inflammatory disorders.

RESULTS

Identification of CNS-9 as a key regulatory element for *Il10* expression in B cells

We began this study by confirming that B cells are the predominant source of IL-10. Single-cell suspensions prepared from the spleen and peritoneal cavity were stimulated with phorbol 12-myristate 13-acetate (PMA) and ionomycin in the presence of protein transport inhibitors (Golgi-Stop and Golgi-Plug) (fig. S1, A to D) (*6*). To identify crucial cis-acting regulatory elements involved in *Il10* transcription in B cells, we used an integrated genome-wide approach, combining ATAC-seq and RNA-seq analyses on publicly available datasets of 11 types of IL-10–producing B cells (Fig. 1A and fig. S2, A and B) (*31*). RNA-seq data revealed different *Il10* expression levels across the 11 types of B cells (Fig. 1B). ATAC-seq data identified open chromatin region (OCR) scores representing chromatin accessibility across the *Il10* locus in these cells. This analysis revealed a total of 33 OCRs (OCR 21025 to OCR 21057), some of which overlapped with previously defined CNSs (Fig. 1C and fig. S2A). To determine potential regulatory elements associated with *Il10* expression, we analyzed the correlation between OCR scores and *Il10* mRNA levels across all 33 OCRs (fig. S2C). This analysis identified 10 OCRs that were significantly correlated with *Il10* expression, 5 of which overlapped with CNSs, whereas the remaining 5 did not (Fig. 1D).

To more precisely identify functional regions regulating *Il10* expression, we cross-analyzed ATAC-seq and ChIP-seq results for p300, DNA looping–related proteins, and histone modifications using publicly available datasets of splenic B cells (*32*–*35*). Notably, CNS-9 exhibited strong enrichment of the enhancer-associated coactivator p300 and key DNA looping–associated proteins, including RAD21, MLL1, and BRG1 (Fig. 1E). In addition, histone modifications indicative of enhancer activity—such as H3K27Ac, H3K4me1, and H3K4me2—were also highly enriched in the CNS-9 region (Fig. 1E). To directly assess whether CNSs have enhancer activity and cooperate with the *Il10* promoter, each CNS region was cloned into the pXPG reporter vector carrying the *Il10* minimal promoter and transfected into A20 cells, a mature B cell line (fig. S3A). Among the areas tested, CNS-9 showed the highest reporter activity compared to other regions, with a 6.8-fold enhancement in reporter activity compared to the condition using only the *Il10* minimal promoter (Fig. 1F). To further evaluate the dependence of CNS-9 activity on position and orientation, we compared reporter constructs in different arrangements relative to the *Il10* minimal promoter. When positioned upstream of the promoter in either forward or reverse orientation, CNS-9 increased luciferase activity to a similar degree, indicating that its activity is orientation independent (fig. S3B). We then tested how its activity depends on position by moving CNS-9 downstream of the luciferase gene. Although the level of enhancement was somewhat reduced compared to the upstream placement, CNS-9 still significantly boosted transcription relative to the minimal promoter alone (fig. S3C). Collectively, these findings show that CNS-9 maintains its enhancer activity across various positions and orientations, confirming its important role as a regulatory element for *Il10* expression in B cells.

NFATc1 regulates *Il10* transcription by controlling the enhancer function of CNS-9

To identify transcription factors responsible for CNS-9-mediated *Il10* expression in B cells, we analyzed publicly available microarray data from 25 types of IL-10–producing B cells (Fig. 2A and fig. S4A). Using motif analysis, we predicted transcription factors likely to bind CNS-9 (fig. S4B). Then, we examined the correlation between the *Il10* expression and expression levels of these transcription factors across the 25 different types of B cells. This analysis identified 12 candidate transcription factors with potential CNS-9 binding activity (Fig. 2B and fig. S4C). To prioritize key regulators, we assessed the absolute expression levels of these candidates. We found that members of the NFAT family—including NFATc1, NFATc2, and NFATc3—were expressed at substantially higher levels than other transcription factors in B cells (Fig. 2C). Notably, we previously reported that NFATc2 binding to CNS-9 induces *Il10* transcription in a T_H2 cell–specific manner (*23*). To investigate whether NFAT regulates *Il10* transcription in B cells, we treated B cells with CsA, a calcineurin inhibitor that blocks NFAT activation. CsA treatment significantly reduced *Il10* mRNA levels in A20 cells and suppressed CNS-9–driven luciferase activity, suggesting that calcineurin-dependent NFAT signaling is a key regulator of *Il10* transcription in B cells (fig. S5, A and B). To determine the critical NFAT isoform, we examined *Il10* mRNA expression levels following the overexpression or knockdown of individual NFAT proteins in A20 cells (fig. S5, C and D). NFATc1 overexpression significantly increased *Il10* mRNA levels, whereas NFATc1 knockdown reduced *Il10* mRNA levels. In contrast, the manipulation of NFATc2 and NFATc3 had minimal effects (Fig. 2, D and E). To gain a broader understanding of NFATc1 function in B cells, we analyzed publicly available microarray data from splenic B cells of *NFATc1*$^{\Delta CD79a}$ mice (*36*). Differential expression analysis revealed widespread transcriptional changes upon NFATc1 deficiency, with 818 genes significantly down-regulated and 662 genes up-regulated compared with wild-type (WT) controls (fig. S6A), suggesting that NFATc1 can both activate and repress gene expression in B cells. Notably, *Il10* was prominently down-regulated within the immune regulation and cytokine category, consistent with our findings that NFATc1 is a critical regulator of *Il10* expression in B cells (fig. S6B). Gene expression profiling further showed coordinated alterations in pathways related to B cell development and activation (*37*–*45*); immune regulation and cytokine (*1*, *46*–*49*); type I interferon–stimulated genes (*50*); and cell adhesion, migration, and trafficking (*51*–*56*) (fig. S6B). Together, these transcriptomic changes highlight NFATc1's broad regulatory role in B cells and suggest that NFATc1 may control *Il10* expression. To examine the functional role of NFAT at CNS-9, we conducted genomic sequence analysis and found four conserved putative NFAT-binding motifs (fig. S7A). Three of these motifs were chosen for functional analysis and were mutated

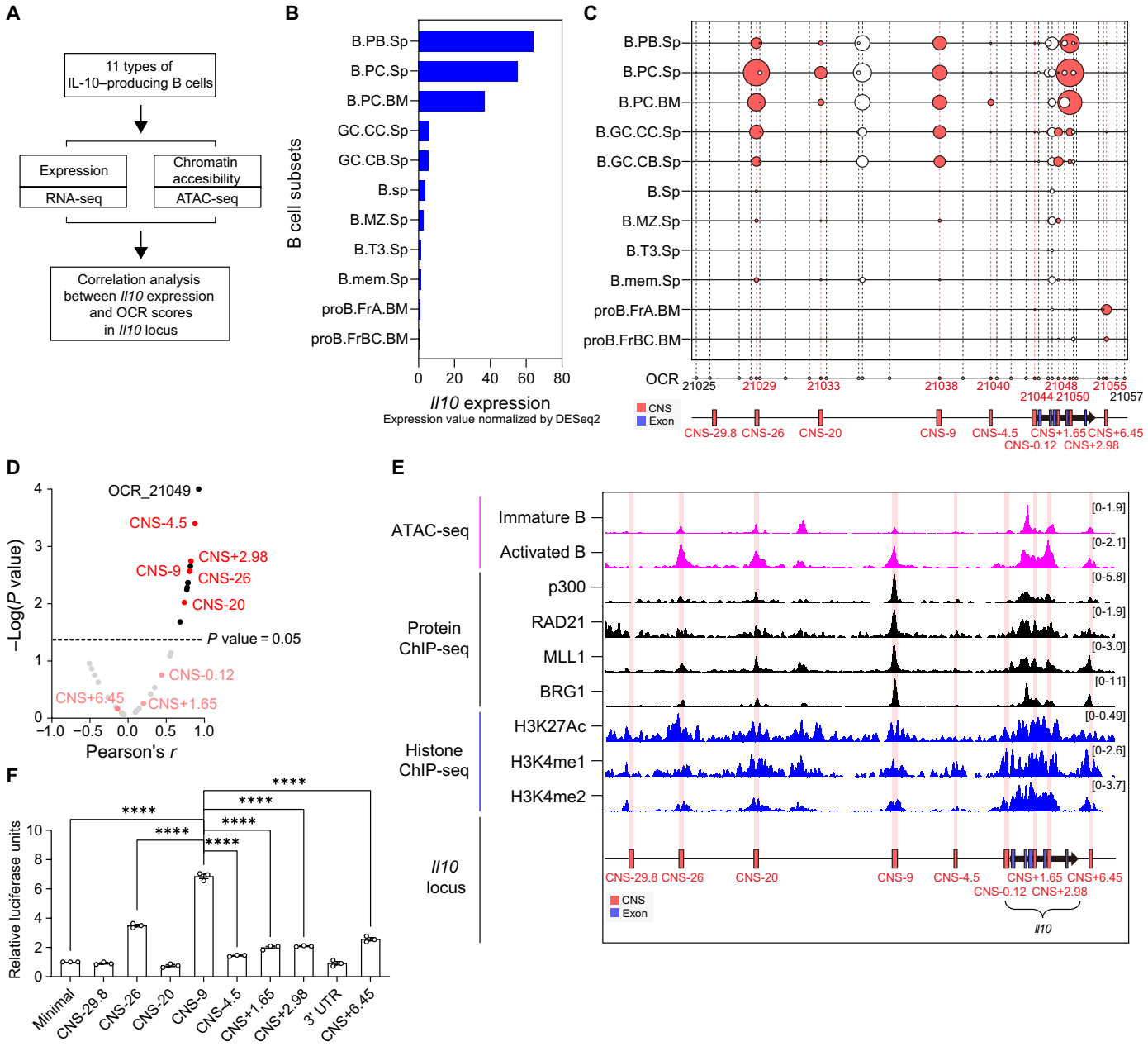

Fig. 1. *Il10* CNS-9 is a key regulatory element for IL-10 expression in B cells. (**A**) Correlation analysis scheme between *Il10* expression and OCR scores in the *Il10* locus. (**B**) *Il10* expression levels across 11 B cell subsets. (**C**) OCR scores of 33 OCR regions in the *Il10* locus across 11 B cell subsets. Circles represent OCRs, with numbers assigned by OCR ID. Red bars mark CNSs, blue bars mark exons, and OCRs overlapping CNSs are highlighted in red. (**D**) Plot of correlations between *Il10* expression and OCR scores. The *x* axis shows Pearson's *r*, and the *y* axis shows $-\log_{10}(P \text{ value})$. A dotted line indicates a *P* value of 0.05, and OCRs corresponding to CNSs are highlighted in red. (**E**) Analysis of ATAC-seq (pink), protein ChIP-seq (black), and histone ChIP-seq (blue) data from public datasets (GSE103057, GSE82144, GSE33819, and GSE92344) in the *Il10* locus of B cells. (**F**) Reporter assay of *Il10* CNSs in A20 cells. Each CNS locus was cloned into the pXPG vector carrying the *Il10* minimal promoter. Results are expressed as relative units compared to the luciferase activity of a pXPG vector containing only the minimal promoter. Data are representative of three independent experiments with similar results. Data are presented as means ± SEM. Statistical analysis was performed using a two-tailed unpaired Student's *t* test. ****$P < 0.0001$.

either individually or in combination within CNS-9 cloned into the pXPG vector. These mutations markedly reduced enhancer activity, with single mutations producing effects similar to the triple mutation (Fig. 2F). Consistently, NFATc1 overexpression strongly enhanced reporter activity from WT CNS-9, but not the mutant construct, confirming that NFATc1 binding is required for CNS-9 enhancer function (Fig. 2G).

To clarify whether NFATc1 acts through CNS-9 rather than the *Il10* minimal promoter, we performed additional reporter assays using distinct promoter contexts. The overexpression of NFATc1 did not increase reporter activity driven by the *Il10* minimal promoter alone (fig. S7B). In contrast, when CNS-9 was linked to an unrelated 31–base pair (bp) minimal promoter in the pGL4.23 backbone,

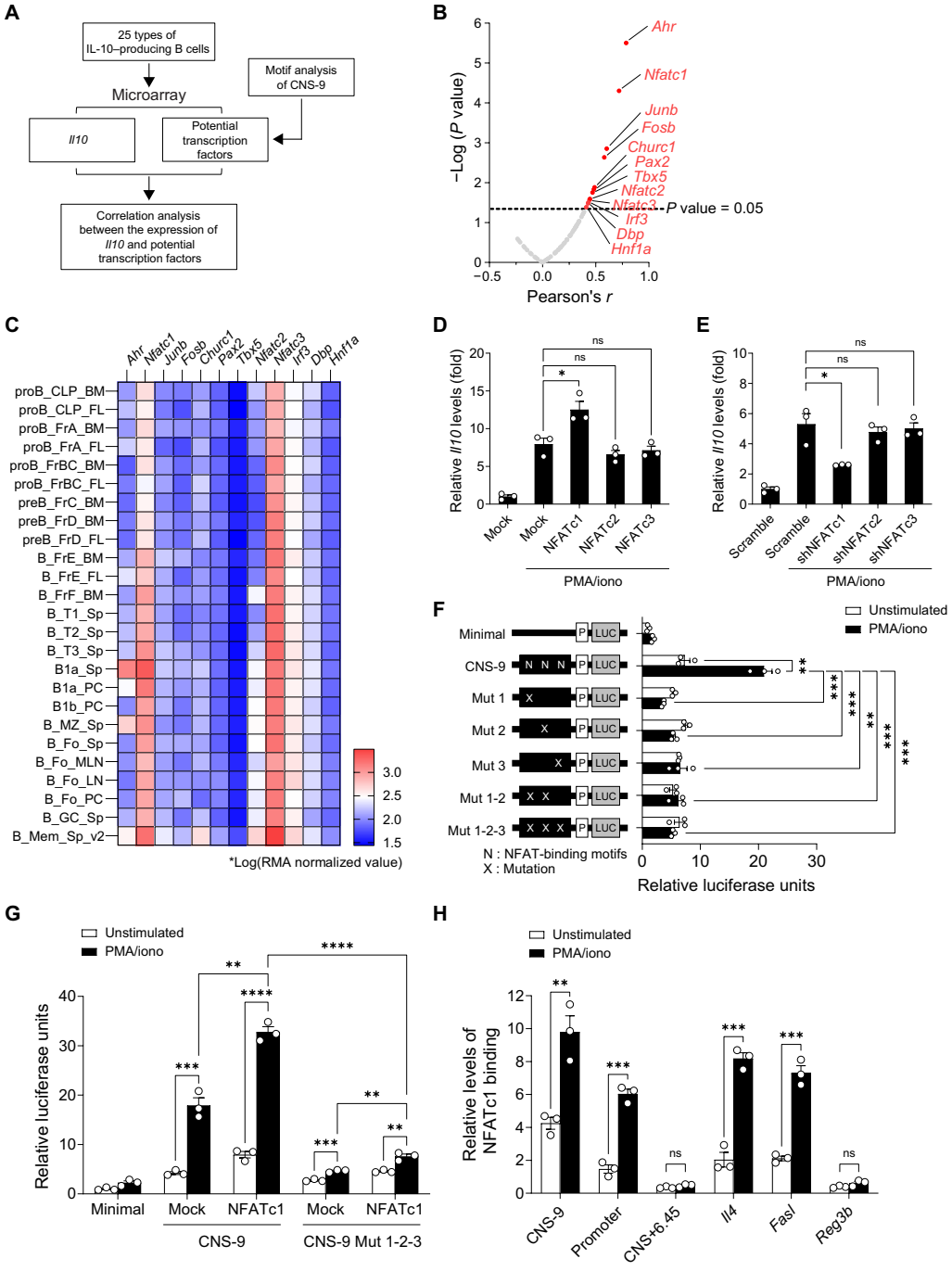

Fig. 2. NFATc1 regulates *Il10* via CNS-9 enhancer in B cells. (**A**) Correlation analysis of *Il10* expression with potential transcription factors using published microarray data; candidates were identified by motif analysis of CNS-9. (**B**) Plot of correlations between the expression levels of *Il10* and potential transcription factors. The *x* axis shows Pearson's *r*, and *y* axis shows $-\log_{10}(P \text{ value})$. A dotted line indicates $P = 0.05$, and significant factors ($P < 0.05$) are highlighted in red. (**C**) Heatmap of expression profiles of 12 candidate transcription factors across 25 IL-10–producing B cell populations, shown in log scale using RMA values. (**D** and **E**) qRT-PCR analysis of *Il10* mRNA in A20 cells transfected with expression (D) or shRNA (E) vectors for NFATc1, NFATc2, and NFATc3. Results are expressed as fold difference relative to *Il10* mRNA levels in unstimulated A20 cells. (**F** and **G**) Luciferase reporter assay in A20 cells transfected with the pXPG vector containing CNS-9. Results are expressed as relative luciferase activity normalized to the unstimulated condition using a vector with only the minimal promoter. (F) Three NFAT motifs in CNS-9 were mutated individually or additively, and N and X denote NFAT-binding motifs and their mutations, respectively. (G) A pXPG vector containing WT or mutated CNS-9 was cotransfected with an NFATc1 expression vector or a mock vector into A20 cells. (**H**) ChIP assay in mouse B cells with anti-NFATc1 antibody. Immunoprecipitated DNA was quantified by qRT-PCR and normalized to input DNA. Relative enrichment was compared with IgG controls. [(D) and (H)] Data are representative of three independent experiments with similar results. Data are presented as means ± SEM. Statistical analysis was performed using a two-tailed unpaired Student's *t* test. **P* < 0.05, ***P* < 0.01, ****P* < 0.001, and *****P* < 0.0001. ns, not significant.

NFATc1 overexpression robustly enhanced luciferase activity, whereas the minimal promoter alone remained unresponsive (fig. S7C). Consistent with these results, mutating all six predicted NFAT-binding motifs within CNS-9 markedly reduced basal enhancer activity and significantly blunted the responsiveness to NFATc1 overexpression compared with WT CNS-9 (fig. S7, D and E). These data indicate that CNS-9 is required for NFATc1-dependent transcriptional activation. To further confirm the direct binding of NFATc1 to CNS-9, we performed a ChIP assay in mouse B cells. Upon PMA and ionomycin stimulation, NFATc1 binding was significantly enriched at the CNS-9 and the *Il10* promoter regions but was undetectable at CNS+6.45 (Fig. 2H). As expected, *Il4* and *Fasl* promoters served as positive controls for NFATc1 binding, while no binding was observed at the *Reg3b* promoter, which is not expressed in B cells (Fig. 2H).

To further confirm the specificity of NFAT binding to CNS-9 and clarify the roles of individual NFAT isoforms, we conducted electrophoretic mobility shift assays (EMSAs) and additional ChIP analyses in mouse B cells. Nuclear extracts from $CD19^+$ B cells stimulated with PMA and ionomycin showed significantly increased binding to DNA probes containing either an NFAT consensus sequence or CNS-9 compared to unstimulated cells (fig. S8A, lanes 1, 2, 5, and 6). This binding was competitively blocked by excess cold oligomers, confirming sequence-specific NFAT-DNA interactions (fig. S8A, lanes 3, 4, 7, and 8). Supershift assays indicated a strong shift with anti-NFATc1 antibody, while anti-NFATc3 had no effect; anti-NFATc2 caused only a modest shift, suggesting that NFATc1 predominantly interacts with CNS-9 in B cells (fig. S8A, lanes 9 to 11). Consistent with these results, a ChIP assay using an anti-NFATc2 antibody showed minimal enrichment at the *Il10* promoter, CNS-9, or CNS+6.45 in both unstimulated and PMA/ionomycin-stimulated B cells (fig. S8B). Alongside our NFATc1 ChIP data (Fig. 2H), these findings demonstrate that NFATc1 is the main NFAT isoform that directly binds to CNS-9 in B cells, while NFATc2 and NFATc3 contribute little or not at all to IL-10 regulation at this locus. These findings show that NFATc1 directly binds to CNS-9 and regulates *Il10* transcription in B cells by modulating the enhancer activity of CNS-9.

NFATc1 mediates intrachromosomal looping between CNS-9 and the *Il10* promoter

Previous studies have shown that distal regulatory elements can physically interact with gene promoters via DNA looping, thereby promoting active transcription (*57*, *58*). To determine whether NFATc1 regulates the chromatin loop formation to enhance *Il10* transcription, we performed chromosome conformation capture (3C) assays. Cross-linked genomic DNA was digested with the restriction enzyme Xba I, which cuts specific sites around the CNS-9 and the *Il10* promoter (fig. S9A). The digested chromatin fragments were subsequently ligated to join DNA elements in close physical proximity, and the relative frequency of ligation was analyzed by quantitative real-time polymerase chain reaction (qRT-PCR) using a unique primer pair. The efficient digestion of restriction sites between fragments A and B was confirmed by Xba I treatment (fig. S9B). As a control, the ligated sample exhibited a significant increase in interaction compared to the unligated sample, confirming the specificity of the assay (fig. S9C). We first analyzed the interactions between the promoter and other DNA loci within the *Il10* gene locus. In B cells, 3C products between the *Il10* promoter (E) and CNS-9 (B) were more abundant than interactions between the promoter and other loci (fig. S9D). We next examined the gene loop formation between CNS-9 and other DNA loci. In B cells, 3C products were enriched between CNS-9 (B) and the promoter (E) (fig. S9E). CNS+6.45 (H) also exhibited interaction with both the promoter (E) and CNS-9 (B) (fig. S9, D and E). These results indicate that the *Il10* promoter is in close spatial proximity to CNS-9 in B cells, thereby facilitating the formation of chromatin looping. To assess the role of NFATc1 in mediating this gene looping, we examined whether NFATc1 regulates this intrachromosomal interaction. The overexpression of NFATc1 significantly enhanced chromatin loop formation between CNS-9 and the *Il10* promoter (fig. S9F). Conversely, NFATc1 knockdown inhibited this interaction (fig. S9G). Together, these results demonstrate that NFATc1 mediates intrachromosomal interactions between CNS-9 and the *Il10* promoter, thereby promoting active *Il10* transcription in B cells.

B1a cells are the primary producers of IL-10 through NFATc1-CNS-9 interaction

Having established the molecular mechanism by which NFATc1 regulates *Il10* expression through chromatin looping, we next sought to identify the specific B cell subpopulation in which this regulatory pathway is most active and physiologically relevant. To this end, we examined IL-10 production across B cell subsets, with particular attention to B1a cells, which are well known as the predominant source of B cell–derived IL-10 (*10*). Among splenic B cells, B1a and marginal zone (MZ) B cells showed the highest levels of IL-10 production (fig. S10, A and E to G), and B1a cells showed markedly higher IL-10 mean fluorescence intensity (MFI) compared to B2 cells (fig. S10B). In the peritoneal cavity, B1a cells were the predominant IL-10 producers, also displaying the highest IL-10 MFI relative to B1b and B2 cells (fig. S10, C and D). These findings indicate that B1a cells are the major source of B cell-derived IL-10.

To determine which B cell subsets require CNS-9 for IL-10 expression, we generated CNS-9 knockout (KO) mice (Fig. 3A) and validated the genotypes of CNS-9 mutant mice by Southern blot and PCR analysis (fig. S11A). To evaluate potential the physiological effects of CNS-9 deletion, we monitored body weight changes and spleen weights in WT and CNS-9 KO mice. No significant differences were observed between the two groups (figs. S11, B to E and S12, A and B). Consistent with these findings, the proportions of naive T cells, effector/memory T cells, and regulatory T cells in the spleen remained unchanged between the two groups (fig. S12, C to F), indicating that CNS-9 deletion does not disrupt the overall growth or T cell homeostasis under steady-state conditions. Moreover, analyses of B cell subtypes in both bone marrow and spleen revealed no significant differences in the frequency of Hardy fractions (fig. S13, A and B) or in the distribution of splenic B cells (fig. S13C). These results suggest that CNS-9 deletion does not affect B cell development, homeostasis, or general physiology.

To investigate cell-intrinsic effects of CNS-9 deficiency, we generated mixed bone marrow chimeric mice by transplanting 1:1 mixtures of congenic WT and CNS-9 KO bone marrow (Fig. 3B). In the spleen, CNS-9 KO cells displayed reduced IL-10 production and lower MFI in B cells (Fig. 3C and fig. S14, A to D), consistent with the role of these cells as a primary source of IL-10 (fig. S1A) (*6*). Notably, other immune cell populations remained unaffected (Fig. 3C and fig. S14, A to D). Among B cell subsets, CNS-9 KO B1a cells, in particular, exhibited a significant reduction in both IL-10 production and MFI (Fig. 3, D and E, and fig. 15, A to G), reinforcing their dependence on CNS-9 for optimal IL-10 expression. This is especially noteworthy given the established role of B1a

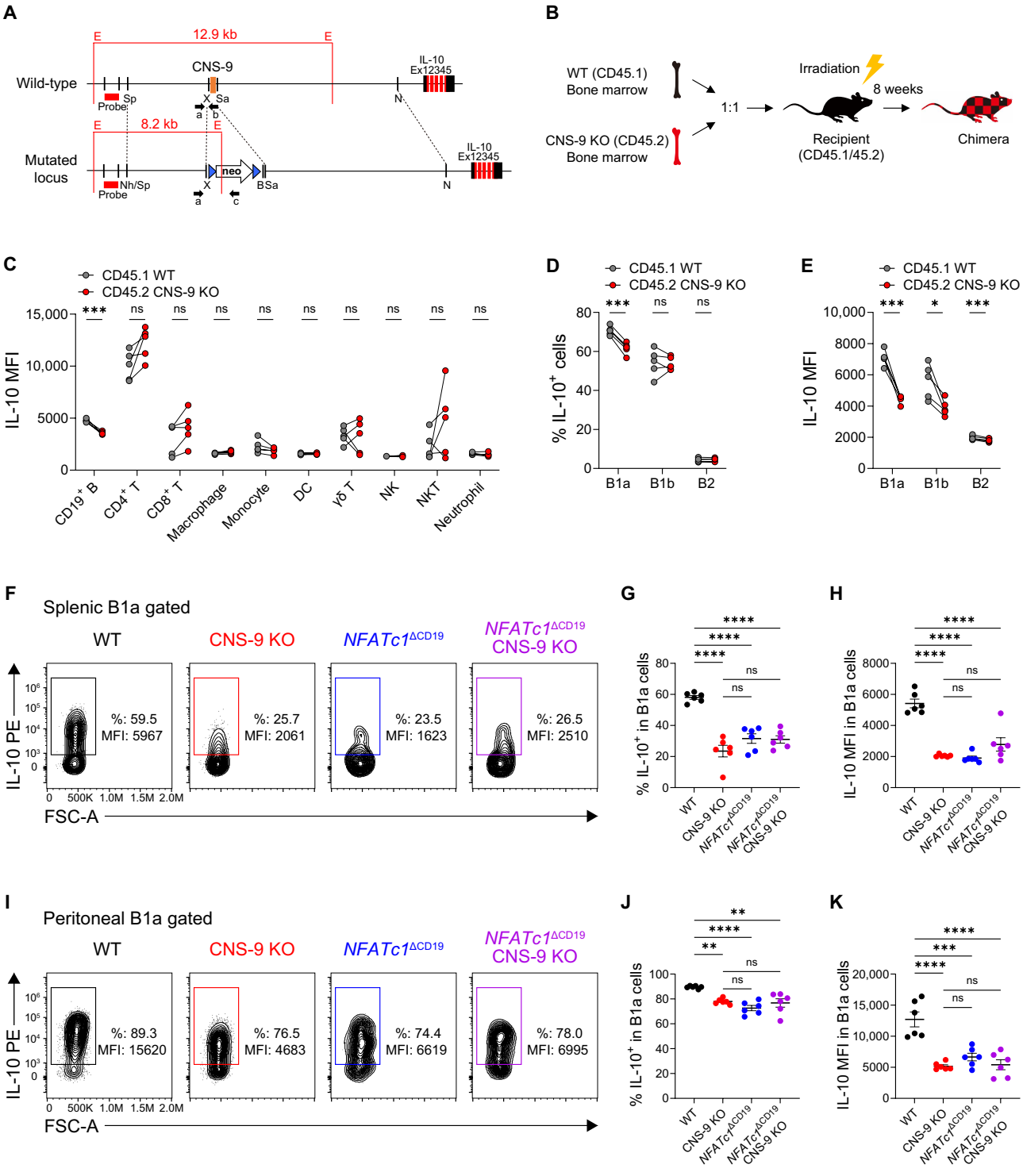

Fig. 3. CNS-9 drives IL-10 production in B1a cells. (**A**) Schematic diagram of CNS-9 KO mice generation. E marks for Eco RI site; a is the forward primer for WT and KO, while b and c are reverse primers for WT and KO, respectively. (**B**) Schematic diagram for generating mixed bone marrow chimeric mice. (**C**) MFI of IL-10$^+$ cells within the indicated cell types in the spleen ($n = 5$ for mixed bone marrow chimeras). (**D** and **E**) Frequency (D) and MFI (E) of IL-10$^+$ cells within B1a, B1b, and B2 cells in the spleen ($n = 5$ for mixed bone marrow chimeras). (**F** to **H**) Representative flow cytometry plots (F), frequency (G), and MFI (H) of IL-10$^+$ cells in splenic B1a cells from each WT and mutant mice ($n = 6$ for WT, CNS-9 KO, *NFATc1*$^{\Delta CD19}$, and *NFATc1*$^{\Delta CD19}$ CNS-9 KO). (**I** to **K**) Representative flow cytometry plots (I), frequency (J), and MFI (K) of IL-10$^+$ cells in peritoneal B1a cells from each WT and mutant mice ($n = 6$ for WT, CNS-9 KO, *NFATc1*$^{\Delta CD19}$, and *NFATc1*$^{\Delta CD19}$ CNS-9 KO). All data are representative of three independent experiments with similar results. Data are presented as means ± SEM. Statistical analysis was performed using a two-tailed paired Student's *t* test [(C) to (E)] or a one-way ANOVA followed by Tukey's post hoc test [(G), (H), (J), and (K)]. *$P < 0.05$, **$P < 0.01$, ***$P < 0.001$, and ****$P < 0.0001$. NK, natural killer; NKT, natural killer T.

cells as a predominant source of B cell–derived IL-10 (fig. S10, A to D) (*10*).

To further define the role of NFATc1-CNS-9 interaction in IL-10 expression in B cells, we generated CD19-Cre *NFATc1*$^{fl/fl}$ (*NFATc1*$^{\Delta CD19}$) mice and CD19-Cre *NFATc1*$^{fl/fl}$ CNS-9 KO (*NFATc1*$^{\Delta CD19}$ CNS-9 KO) mice. We then compared IL-10 production in B1a cells from WT, CNS-9 KO, *NFATc1*$^{\Delta CD19}$, and *NFATc1*$^{\Delta CD19}$ CNS-9 KO mice in both the spleen and peritoneal cavity. In all three mutant strains, the frequency of IL-10^{+} B1a cells and IL-10 MFI were significantly reduced in the spleen and peritoneal cavity compared to WT mice (Fig. 3, F to K). Moreover, there was no significant difference in IL-10 levels among the three mutant strains CNS-9 KO, *NFATc1*$^{\Delta CD19}$, and *NFATc1*$^{\Delta CD19}$ CNS-9 KO (Fig. 3, F to K), suggesting that NFATc1-mediated CNS-9 regulation is essential for B1 cell–derived IL-10 production in both compartments.

NFATc1-CNS-9 signaling drives IL-10 expression to limit sepsis inflammation

To investigate the role of NFATc1-mediated CNS-9 regulation in IL-10 expression and its impact on inflammatory responses, we assessed the susceptibility of CNS-9 KO, *NFATc1*$^{\Delta CD19}$, and *NFATc1*$^{\Delta CD19}$ CNS-9 KO mice to LPS-induced sepsis (Fig. 4A). All three mutant strains showed significantly reduced survival rates compared to WT, with no significant differences among the mutant groups (Fig. 4B). The histopathological analysis of the lungs and liver revealed severe tissue damage in mutant mice (Fig. 4C and fig. S16, A and B). Lung sections showed extensive neutrophil infiltration, alveolar hemorrhage, and edema accompanied by thickened alveolar septa. Similarly, liver sections of mutant mice showed extensive hepatic injury, characterized by hepatocyte necrosis, sinusoidal congestion, and inflammatory cell infiltration. Consistent with these pathological findings, IL-10 production and IL-10 MFI levels in B1a cells were significantly reduced in both the spleen and peritoneal cavity of mutant mice (Fig. 4, D to I, and fig. S16C), demonstrating that NFATc1-mediated activation of CNS-9 is essential for optimal IL-10 expression in B cells. To determine whether reduced IL-10 production by B cells is reflected at the systemic level, we measured total serum IL-10 concentrations following LPS challenge. Consistent with impaired B cell IL-10 production, CNS-9 KO mice exhibited significantly lower serum IL-10 levels than WT controls at 6 hours after intraperitoneal injection of LPS (5 mg/kg) and at both 2 and 6 hours after intraperitoneal injection of LPS (30 mg/kg) (fig. S16, D and E). These findings indicate that CNS-9 deficiency results in a global reduction of circulating IL-10 during endotoxemia. Previous studies have shown that the immunosuppressive effects of IL-10 depend on IL-10 receptor signaling in macrophages and neutrophils, rather than in T or B cells (*59*). Accordingly, we examined how reduced IL-10 production in B cells affects inflammatory cytokine responses in macrophages and neutrophils. Reflecting impaired IL-10–mediated regulation, mutant mice exhibited markedly elevated proinflammatory cytokine levels, with significantly increased IL-6 and IL-1β production in neutrophils and macrophages compared to WT controls (Fig. 4, J to M, and fig. S16F). Serum IL-6 levels were substantially higher in mutant mice, indicating an exacerbated systemic inflammatory response (Fig. 4N). In contrast, phosphate-buffered saline (PBS)–treated WT and mutant mice showed no significant differences in IL-6 or IL-1β production by neutrophils and macrophages, confirming that these elevated cytokine responses are specific to the inflammatory challenge (fig. S16, G to J). Collectively, these findings support a critical role for NFATc1-mediated regulation of CNS-9 in promoting IL-10 expression in B cells and limiting excessive proinflammatory responses during LPS-induced sepsis.

Adoptive transfer of WT B1a cells restores protection against LPS-induced sepsis in CNS-9 KO mice

To verify the protective role of CNS-9–dependent IL-10 in B cells in the LPS-induced sepsis model, we performed adoptive transfer experiments to directly assess its causal contribution to survival and inflammation. The fluorescence-activated cell sorting (FACS)–sorted IL-10–competent WT CD45.1^{+} B1a cells were adoptively transferred into WT or CNS-9 KO recipients before LPS challenge (Fig. 5A and fig. S17A). Transfer of WT B1a cells significantly improved the survival rate of CNS-9 KO mice after intraperitoneal injection of LPS (30 mg/kg), whereas PBS-treated CNS-9 KO mice remained highly vulnerable to lethal sepsis (Fig. 5B). The histopathological analysis of lung and liver tissues showed that adoptive transfer of WT B1a cells significantly reduced tissue damage in CNS-9 KO recipients, including less neutrophil infiltration, alveolar hemorrhage, and hepatic injury (Fig. 5C and fig. S17, B and C). Flow cytometric analysis further revealed that the adoptive transfer of WT B1a cells significantly reduced inflammatory cytokine production in innate immune cells. The proportions of IL-6^{+} and IL-1β^{+} neutrophils and macrophages in the spleen were markedly increased in PBS-treated CNS-9 KO mice but returned toward WT levels after B1a cell transfer (Fig. 5, D to G). In addition, serum IL-6 levels, which were notably elevated in CNS-9 KO mice, were significantly decreased following adoptive transfer of WT B1a cells (Fig. 5H). Together, these findings demonstrate a causal role for CNS-9–dependent IL-10 production by B1a cells in suppressing systemic inflammation and enhancing survival during LPS-induced sepsis.

CNS-12, the human homolog of murine CNS-9, drives NFATc1-dependent IL-10 expression in B cells

Given the conserved nature of CNS-9, we identified a homologous region ~12-kb upstream of the human *IL10* transcription start site, which we designated as CNS-12. To explore its functional role, we analyzed ChIP-seq data from publicly available datasets of human immortalized B cell lines (*60*). CNS-12 exhibited strong enrichment of enhancer-associated markers, including the coactivator p300 and histone modifications H3K27Ac and H3K4me1 (Fig. 6A), both of which are characteristic of active enhancer regions. Notably, NFATc1 binding was also enriched at this locus, suggesting its involvement in regulating human *IL10* gene expression (Fig. 6A). To assess whether CNS-12 physically interacts with the *IL10* promoter, we examined Hi-C data from publicly available datasets (*61*). The analysis revealed significant chromatin interactions between CNS-12 and the human *IL10* promoter region, indicating potential gene regulation through chromatin looping mechanisms (Fig. 6A). To directly evaluate the enhancer activity of CNS-12, we used CRISPR-Cas9 genome editing in Raji B cells to target NFAT-binding motifs within this region (Fig. 6B and fig. S18A). Following electroporation with vectors expressing Cas9 and specific single guide RNAs (sgRNAs) (sgRNA1 and sgRNA2), CRISPR-mediated deletions were confirmed by Sanger sequencing, and mutation profiles were further characterized using Synthego Inference of CRISPR Edits (ICE) analysis. ICE analysis confirmed that CRISPR-mediated targeting of NFAT-binding motifs was efficient, with an average indel frequency of 76.3% for sgRNA1 and 34.7% for sgRNA2 (fig. S18, B and C). The disruption of NFAT-binding motifs significantly reduced *IL10* mRNA levels as determined by qRT-PCR (Fig. 6C). A decrease in

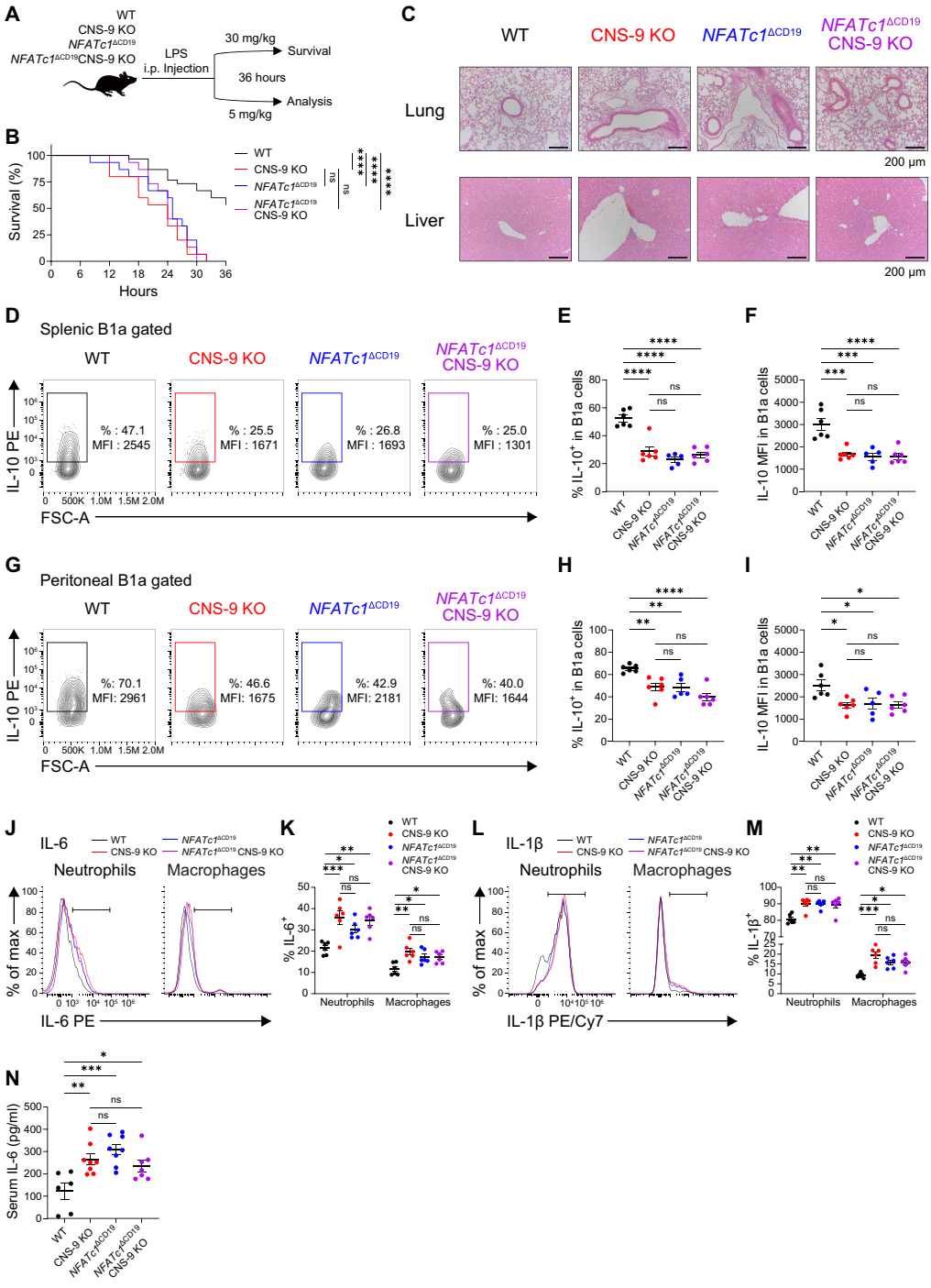

Fig. 4. NFATc1–CNS-9–driven IL-10 production protects against LPS-induced sepsis. (**A**) Schematic diagram of LPS-induced sepsis models. (**B**) Kaplan-Meier survival curve following intraperitoneal (i.p.) injection of LPS (30 mg/kg), monitored for 36 hours ($n = 30$ for WT, $n = 15$ for CNS-9 KO, *NFATc1*$^{\Delta CD19}$, and *NFATc1*$^{\Delta CD19}$ CNS-9 KO). (**C**) Lung and liver sections stained with hematoxylin and eosin. (**D** to **F**) Representative flow cytometry plots (D), frequency (E), and MFI (F) of IL-10$^+$ cells in splenic B1a cells ($n = 6$ for WT, $n = 6$ for CNS-9 KO, $n = 5$ for *NFATc1*$^{\Delta CD19}$, and $n = 6$ for *NFATc1*$^{\Delta CD19}$ CNS-9 KO). (**G** to **I**) Representative flow cytometry plots (G), frequency (H), and MFI (I) of IL-10$^+$ cells in B1a cells from the peritoneal cavity ($n = 6$ for WT, $n = 6$ for CNS-9 KO, $n = 5$ for *NFATc1*$^{\Delta CD19}$, and $n = 6$ for *NFATc1*$^{\Delta CD19}$ CNS-9 KO). (**J** to **K**) Representative histograms (J) and frequency (K) of IL-6$^+$ cells in splenic neutrophils and macrophages ($n = 6$ for WT, CNS-9 KO, *NFATc1*$^{\Delta CD19}$, and *NFATc1*$^{\Delta CD19}$ CNS-9 KO). (**L** and **M**) Representative histograms (L) and frequency (M) of IL-1β$^+$ cells in splenic neutrophils and macrophages ($n = 6$ for WT, CNS-9 KO, *NFATc1*$^{\Delta CD19}$, and *NFATc1*$^{\Delta CD19}$ CNS-9 KO). (**N**) Serum IL-6 concentration ($n = 6$ for WT, $n = 8$ for CNS-9 KO, $n = 8$ for *NFATc1*$^{\Delta CD19}$, and $n = 7$ for *NFATc1*$^{\Delta CD19}$ CNS-9 KO). Data are pooled from three (B) or two independent experiments (N) or are representative of three independent experiments with similar results [(E), (F), (H), (I), (K), and (M)]. Data are presented as means ± SEM. Statistical analysis was performed using log-rank (Mantel-Cox) test (B) and one-way ANOVA followed by Tukey's post hoc test [(E), (F), (H), (I), (K), (M), and (N)]: *$P < 0.05$, **$P < 0.01$, ***$P < 0.001$, and ****$P < 0.0001$. PE, phycoerythrin; FSC, forward scatter.

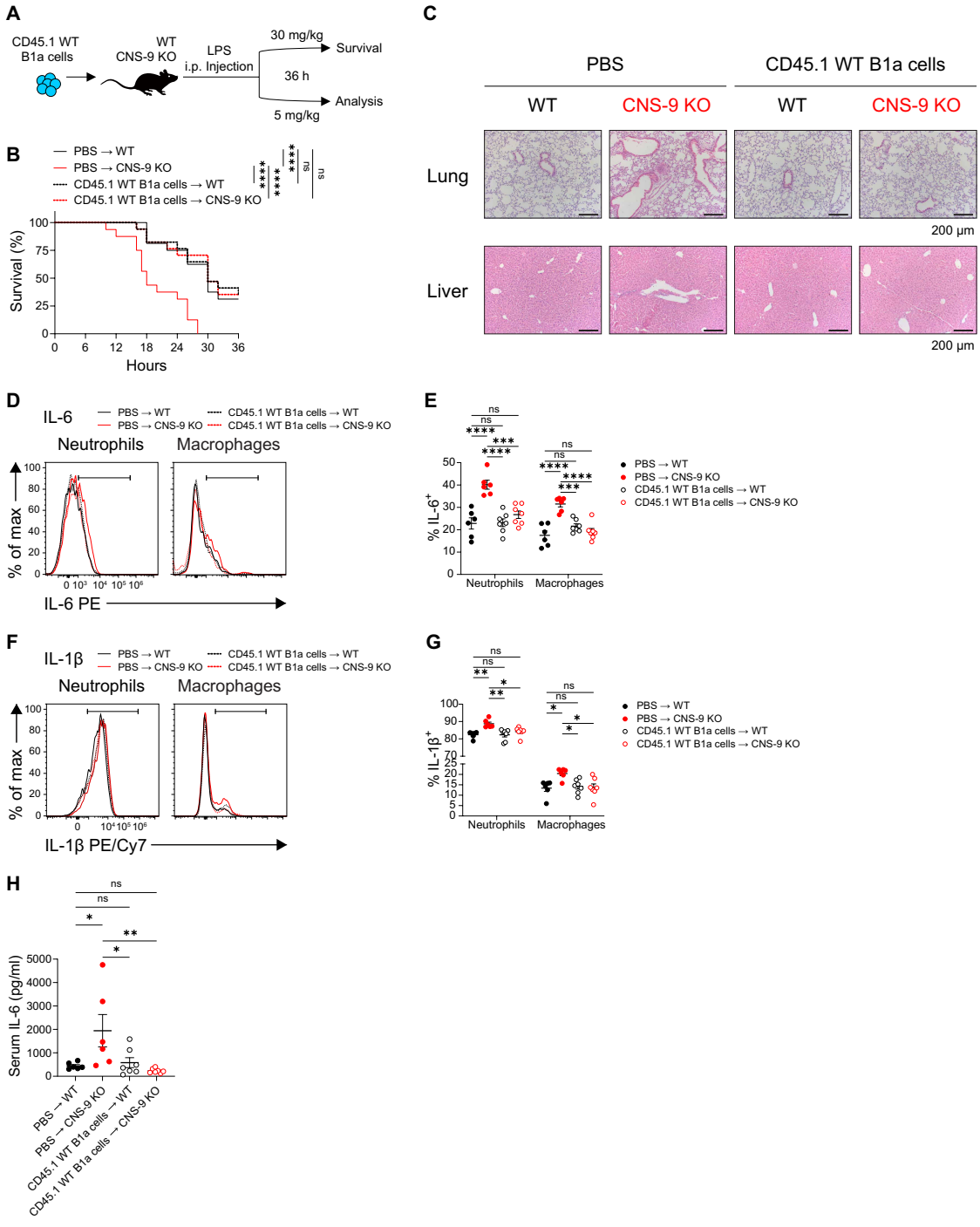

Fig. 5. Adoptive transfer of WT B1a cells mitigates LPS-induced sepsis. (**A**) Schematic diagram of adoptive transfer of B1a cells in the LPS-induced sepsis model. (**B**) Kaplan-Meier survival curve following intraperitoneal injection of LPS (30 mg/kg), monitored for 36 hours ($n = 16$ for PBS → WT and PBS → CNS-9 KO; $n = 17$ for CD45.1 WT B1a cells → WT and CD45.1 WT B1a cells → CNS-9 KO). (**C**) Lung and liver sections stained with hematoxylin and eosin. (**D** and **E**) Representative histograms (D) and frequency (E) of IL-6$^+$ cells in splenic neutrophils and macrophages ($n = 6$ for PBS → WT and PBS → CNS-9 KO; $n = 7$ for CD45.1 WT B1a cells → WT and CD45.1 WT B1a cells → CNS-9 KO). (**F** and **G**) Representative histograms (F) and frequency (G) of IL-1β$^+$ cells in splenic neutrophils and macrophages ($n = 6$ for PBS → WT and PBS → CNS-9 KO; $n = 7$ for CD45.1 WT B1a cells → WT and CD45.1 WT B1a cells → CNS-9 KO). (**H**) Serum IL-6 concentration ($n = 6$ for PBS → WT and PBS → CNS-9 KO; $n = 7$ for CD45.1 WT B1a cells → WT and CD45.1 WT B1a cells → CNS-9 KO). Data are pooled from three (B) or are representative of three independent experiments with similar results [(E), (G), and (H)]. Data are presented as means ± SEM. Statistical analysis was performed using log-rank (Mantel-Cox) test (B) and one-way ANOVA followed by Tukey's post hoc test [(E), (G), and (H)]: *$P < 0.05$, **$P < 0.01$, ***$P < 0.001$, and ****$P < 0.0001$.

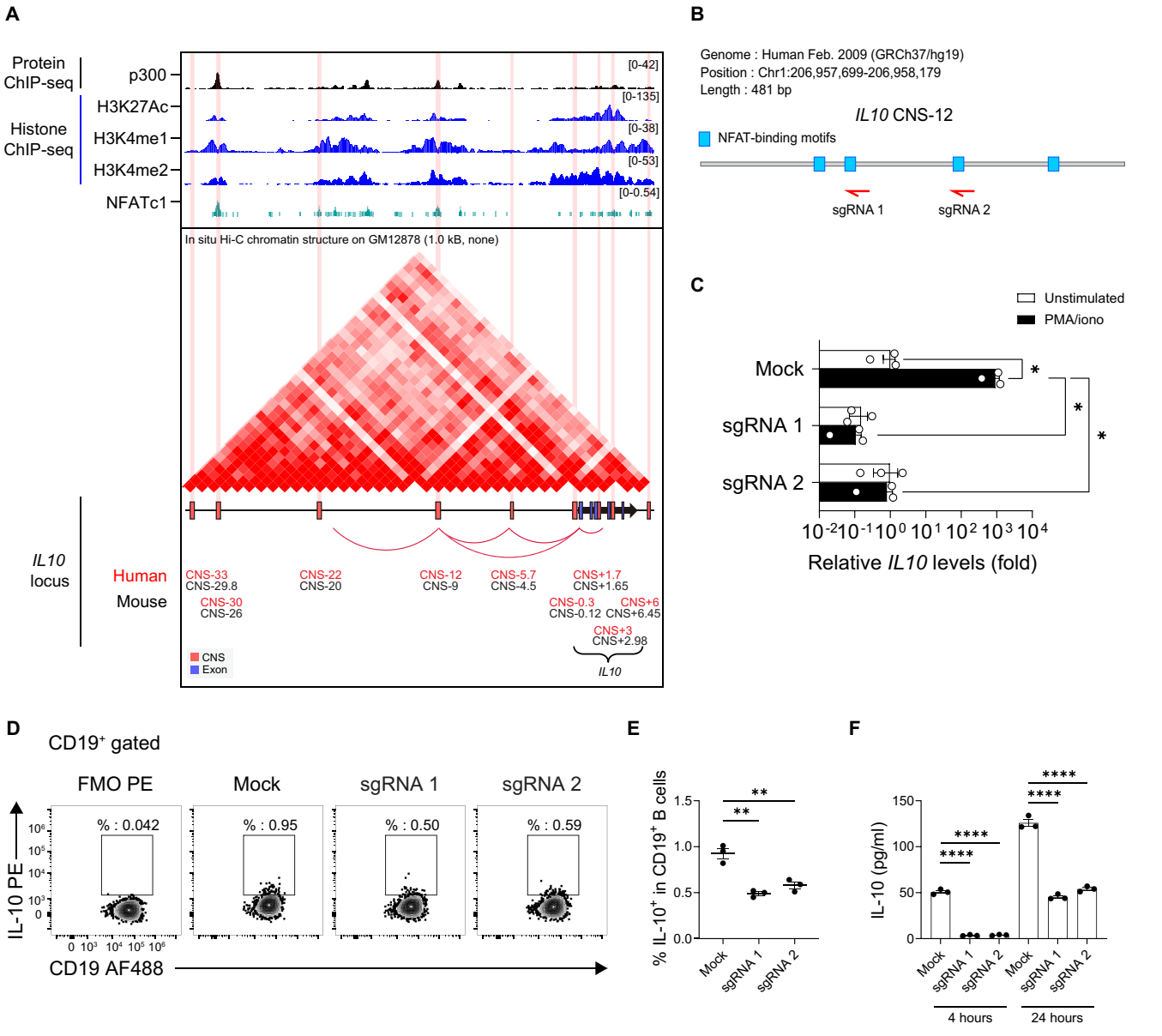

Fig. 6. CNS-12, the human homolog of CNS-9, regulates IL-10 production in human B cells. (**A**) Analysis of ChIP-seq data of p300 (black), histone (blue), NFATc1 (green), and in situ Hi-C data at the *IL10* locus using public datasets (GSE32465, GSE29611, and GSE63525) of GM12878 human immortalized B cells. (**B** to **E**) Raji B cells were electroporated with vectors expressing Cas9 and sgRNAs targeting NFAT- binding motifs in *IL10* CNS- 12 or mock vectors. (B) Schematic diagram of the NFAT- binding motifs in *IL10* CNS-12, identified with rVISTA (Transfac matrices, similarity score of 0.85). Red arrows indicate sgRNA targeting sites. (C) qRT-PCR analysis of *IL10* mRNA in electroporated human Raji B cells, expressed as fold change relative to unstimulated cells. [(D) and (E)] Representative flow cytometry plots (D) and frequency (E) of IL-10$^+$ cells in Raji B cells ($n = 3$ for mock, sgRNA 1, and sgRNA 2). A FMO control for IL- 10 is shown in (D). (**F**) IL- 10 concentrations in culture supernatants of Raji B cells measured at 4 and 24 hours ($n = 3$ for mock, sgRNA 1, and sgRNA 2). Data are pooled from three independent experiments [(C), (E), and (F)]. Data are presented as means ± SEM. Statistical analysis was performed using a two-tailed unpaired Student's *t* test [(C), (E), and (F)]: *$P < 0.05$, **$P < 0.01$, and ****$P < 0.0001$.

IL-10 production was measured by FACS analysis, with appropriate fluorescence-minus-one (FMO) controls confirming the specificity of IL-10 staining (Fig. 6, D and E, and fig. S18D). To further validate the functional impact of CNS-12 disruption, secreted IL-10 levels in culture supernatants were measured by enzyme-linked immunosorbent assay (ELISA). Consistent with the reduced intracellular IL-10 signal, CRISPR-mediated disruption of CNS-12 significantly decreased IL-10 concentrations in the supernatant at both 4 and 24 hours of culture in cells edited with sgRNA1 and sgRNA2 compared with mock controls (Fig. 6F). Collectively, these findings demonstrate that CNS-12, the human homolog of murine CNS-9, functions as an NFATc1-dependent enhancer and plays a critical role in regulating IL-10 expression in human B cells.

DISCUSSION

B cells are major producers of IL-10 and play a crucial role in immune regulation, yet the molecular mechanisms controlling IL-10

expression in B cells remain incompletely understood (*6*–*9*). In this study, we identified NFATc1 as a critical regulator of *Il10* transcription through its direct binding to the CNS-9 enhancer element. This enhancer-dependent regulatory mechanism enables B cells to restrain excessive inflammatory responses during sepsis. We further demonstrated that CNS-12, the human homolog of murine CNS-9, preserves this regulatory function, ensuring the proper expression of IL-10 in human B cells. Collectively, our findings reveal an evolutionarily conserved, enhancer-based mechanism for IL-10 regulation, highlighting the translational relevance of the NFATc1-CNS-9 axis in B cell–mediated immunoregulation.

Through an integrated genomic approach that combined ATAC-seq, RNA-seq, and ChIP-seq analyses, we identified CNS-9 as a key regulatory element for *Il10* expression in B cells. CNS-9 exhibited hallmarks of an active enhancer, including open chromatin configuration, enrichment of p300 coactivator, recruitment of DNA looping–associated proteins (RAD21, MLL1, and BRG1), and deposition of active histone modifications (H3K27Ac, H3K4me1, and H3K4me2). Reporter assay further demonstrated that CNS-9 robustly activates the *Il10* promoter, establishing its function as a bona fide enhancer for B cell–derived IL-10.

We identified NFATc1 as the principal transcription factor that binds to CNS-9 and drives IL-10 expression in B cells. Multiple lines of evidence support this conclusion: (i) NFATc1 is the most abundantly expressed candidate among potential CNS-9–binding transcription factors in IL-10–producing B cells; (ii) pharmacological inhibition of NFAT activation with CsA markedly reduces *Il10* expression; (iii) NFATc1 knockdown or overexpression correspondingly decreases or increases *Il10* mRNA levels; (iv) mutation of NFAT motifs within CNS-9 abolishes its enhancer activity; (v) ChIP assays demonstrate direct binding of NFATc1 to CNS-9 in B cells; and (vi) in vivo, IL-10 production by B1a cells in *NFATc1*$^{\Delta CD19}$ CNS-9 KO mice is reduced to levels comparable to those observed in CNS-9 KO or *NFATc1*$^{\Delta CD19}$ mice. Notably, while NFATc2 has been implicated in IL-10 regulation in T_H2 cells via CNS-9 binding (*23*), our data indicate that NFATc1 is the predominant NFAT family member controlling IL-10 expression in B cells. This finding suggests that cell type–specific utilization of distinct NFAT isoforms regulates the same target gene, revealing an additional layer of complexity in the transcriptional control of *Il10*.

The mutation of any single NFAT-binding motif within CNS-9 causes a near-complete loss of enhancer activity, suggesting that these motifs work together rather than redundantly. Closely spaced transcription factor (TF)–binding sites can improve binding affinity, specificity, and transcriptional output by stabilizing TF interactions with regulatory elements, a phenomenon seen across various enhancers and TF families (*62*, *63*). Therefore, the three NFAT motifs within CNS-9 likely form a cooperative cluster, such that disrupting any one site weakens NFATc1 binding and impairs enhancer function. In addition, NFAT is known to interact with other factors, such as CCAAT/enhancer-binding protein (C/EBP) or activator protein 1 (AP-1), to form ternary complexes that potentiate transcriptional activation (*28*, *64*). Although additional cofactors at CNS-9 remain to be defined, these observations support a model in which CNS-9 activity depends on a cooperative enhancer architecture that renders individual NFAT sites functionally interdependent.

3C assays revealed that NFATc1 mediates chromatin looping between the CNS-9 and *Il10* promoter in B cells, providing a mechanistic basis for the enhancer activity of CNS-9. Enhancer-promoter interaction through chromatin looping is a well-established mechanism for gene activation in various contexts (*57*, *58*). Consistent with this model, NFATc1 overexpression increased, while its knockdown reduced, CNS-9–promoter interaction, suggesting that NFATc1 not only functions as a conventional transcription factor but also plays a role in shaping the three-dimensional chromatin architecture of the *Il10* locus. Nonetheless, the 3C assay used in this study has technical limitations. Cross-linked genomic DNA was digested with Xba I, which selectively cleaves the regions surrounding CNS-9 and the *Il10* promoter, allowing the detection of interactions between these two sites. The absence of Xba I restriction sites around other potential interacting elements, such as CNS-26 and CNS+1.65 or CNS+2.98, precluded the assessment of long-range chromatin interactions involving these regions. Further studies using alternative restriction enzymes or higher-resolution techniques such as 4C or Hi-C will be required to comprehensively map the chromatin interactions across the *Il10* locus.

As previously reported (*10*), our findings confirmed B1a cells as the predominant source of B cell–derived IL-10, and we demonstrated that NFATc1–CNS-9 regulation is essential for IL-10 production in this subset. B1a cells are a distinct B cell population with innate-like properties that reside primarily in the peritoneal cavity and, to a lesser extent, in the spleen (*10*, *65*). They contribute substantially to IL-10 production during infection and inflammation (*11*, *12*). Our study provides a molecular explanation for this high IL-10 expression in B1a cells, highlighting the critical role of NFATc1–CNS-9 interaction. The significant reduction of IL-10 in B1a cells from CNS-9 KO, *NFATc1*$^{\Delta CD19}$, and *NFATc1*$^{\Delta CD19}$ CNS-9 KO mice, with no additive decrease in the double KO, demonstrates that NFATc1 and CNS-9 function within the same pathway to control IL-10 expression. The biological significance of the NFATc1–CNS-9 axis was further demonstrated in an LPS-induced sepsis model, in which all three mutant strains (CNS-9 KO, *NFATc1*$^{\Delta CD19}$, and *NFATc1*$^{\Delta CD19}$ CNS-9 KO) exhibited reduced survival, exacerbated tissue damage, diminished IL-10 production, and elevated proinflammatory cytokines compared with WT controls. These findings underscore the essential role of B cell–derived IL-10 in restraining excessive inflammation during sepsis and establish NFATc1–CNS-9 interaction as a critical mechanism in this process. NFATc1 is required for the development of both B1 and B2 cells (*27*), and B1a cells in particular have been identified as key mediators of protection in sepsis models (*12*, *66*). In this context, our results suggest that B1a cell–derived IL-10 is likely the predominant contributor to the observed protective effects, rather than potential contributions from B2 cells. Thus, the NFATc1–CNS-9 axis appears to be particularly crucial for maintaining IL-10 production in B1a cells during systemic inflammation. Given the high mortality and limited treatment options associated with sepsis, targeting this regulatory pathway represents promising therapeutic potential.

CNS-9 primarily regulates cell-intrinsic IL-10 production in B1a cells, while IL-10 itself can exert cell-extrinsic effects that partially preserve the IL-10$^+$ B1a pool in mixed chimeras. Although CNS-9 deficiency reduced IL-10 expression levels per cell, reflected by decreased IL-10 MFI, the frequency of IL-10$^+$ B1a cells was only modestly reduced in mixed chimeras but sharply diminished in full KO mice. This discrepancy suggests that CNS-9 may primarily control cell-intrinsic IL-10 production, while cell-extrinsic signals may partially preserve the IL-10$^+$ B1a population in a mixed cellular environment. One plausible explanation is that IL-10 produced by WT cells in chimeric mice provides paracrine support that promotes the maintenance or stabilization of IL-10–producing B1a cells, consistent with previous reports describing autocrine and paracrine roles

of IL-10 in B-cell activation, survival, and differentiation (*1*, *67*–*72*). Although the reduction in IL-10–producing B1a cells and IL-10 expression levels in CNS-9 KO mice was moderate at the cellular level, these changes were accompanied by markedly exacerbated inflammatory responses and reduced survival during sepsis. This observation suggests that even moderate alterations in enhancer activity can produce disproportionately large effects on inflammatory outcomes, particularly for genes such as *Il10* that function as central nodes in immunoregulatory networks. Although IL-10 is produced by multiple immune cell types—including $CD4^+$ T cells, macrophages, and neutrophils—several observations suggest a preferential role for B1a cell–derived IL-10 in this model. Our comparative analysis showed that B cells constitute the largest fraction of $IL\text{-}10^+$ leukocytes, with B1a cells representing the major IL-10–producing subset and displaying high IL-10 expression levels. Despite comparable frequencies of IL-10–producing $CD4^+$ T cells and myeloid populations between WT and CNS-9 KO mice, total circulating IL-10 concentrations were significantly reduced in CNS-9 KO mice during endotoxemia, indicating that CNS-9–dependent B cell IL-10 substantially contributes to systemic IL-10 availability. This interpretation is consistent with previous studies showing that B1a-deficient mice develop exacerbated sepsis despite the presence of other IL-10–producing immune cells (*12*). Together with our adoptive transfer experiments, these findings support a model in which B1a cell–derived IL-10 acts as a key early regulator that restrains excessive inflammatory responses, although contributions from other IL-10–producing cell types are not excluded.

Extending these findings to human B cells, we demonstrated that these regulatory mechanisms identified in mouse B cells are conserved in humans. The human homolog of murine CNS-9, designated CNS-12, exhibits similar enhancer features, including p300 enrichment, active histone modifications, and NFATc1 binding. Moreover, Hi-C analysis revealed significant interactions between CNS-12 and the *IL10* promoter, indicating the conservation of chromatin looping. Functional validation using CRISPR-Cas9-mediated disruption of NFAT binding motifs within CNS-12 confirmed its essential role in IL-10 expression in human B cells. Together, these findings suggest that the NFATc1-CNS-9/12 regulatory axis represents a fundamental and evolutionarily conserved mechanism for controlling IL-10 expression in B cells.

CNSs are increasingly recognized as key elements of gene regulatory regions and often harbor disease-associated single-nucleotide polymorphisms (SNPs) (*73*–*75*). Notably, SNPs such as rs3024505, rs3024493, and rs11119570 in the *IL10* regulatory landscape are located within CNS+6 (corresponding to mouse CNS+6.45), CNS+1.7 (mouse CNS+1.65), and CNS-22 (mouse CNS-20), respectively, implicating these regions as potential modulators of IL-10 expression in immune-related conditions (*76*–*78*). CNS-12 in the human *IL10* gene locus, despite its high sequence conservation and homology to mouse CNS-9, has not been reported to contain any risk SNPs. Nevertheless, our findings suggest that CNS-12 plays a regulatory role in IL-10 expression, particularly in B1a cells during sepsis. Further investigation of CNS-12, as well as other regions such as CNS+6, CNS+1.7, and CNS-22, which harbor risk SNPs, will be necessary to clarify how these regulatory elements contribute to IL-10–mediated immune homeostasis and disease pathogenesis.

While this study emphasizes the central role of CNS-9 in regulating IL-10 expression in B cells, additional cis-regulatory elements are likely involved. Correlation analysis between OCR scores and *Il10* mRNA levels across 33 OCRs in 11 B cell subsets identified five OCRs overlapping with CNSs: CNS-26, CNS-20, CNS-4.5, CNS+2.98, and CNS-9. OCR_21049, although not evolutionarily conserved, exhibited a significant correlation with *Il10* expression, suggesting potential functional relevance. Reporter assays further supported this possibility: CNS-9 exhibited the highest reporter activity, while CNS-26, CNS-4.5, CNS+1.65, CNS+2.98, and CNS+6.45 also significantly enhanced luciferase activity compared with a minimal promoter control. Consistent with these findings, ChIP-seq data revealed strong p300 enrichment at CNS-9 and enrichment of DNA-looping proteins and active histone marks at other CNSs, including CNS-26, CNS-20, CNS+1.65, CNS+2.98, and CNS+6.45. Furthermore, 3C assays provided direct evidence of physical interactions between the *Il10* promoter and these regulatory elements. Although the interaction between the *Il10* promoter and CNS-9 was most prominent, we also detected promoter interactions with CNS+6.45 and evidence of looping between CNS-9 and CNS+6.45. These results suggest that IL-10 expression in B cells is coordinated not only by individual CNSs but also through cooperative interactions among multiple cis-regulatory elements.

Our findings have several implications for understanding the regulation of immune homeostasis and guiding the development of treatments. First, we identified a specific enhancer-transcription factor interaction, NFATc1 binding to CNS-9/12, which could be targeted to control B cell–derived IL-10 production in inflammatory disorders. Enhancing this interaction might help reduce inflammation in autoimmune diseases, while inhibiting it could benefit conditions such as chronic infections or cancers, where excessive IL-10 promotes pathogen persistence or tumor immune evasion. Second, these results underscore the importance of cell type–specific regulatory mechanisms in controlling cytokine expression, a key consideration for designing precisely targeted immunomodulatory therapies. Last, the conservation of this regulatory pathway between mice and humans underscores its potential for translation, making NFATc1–CNS-9/12 a promising therapeutic target.

Several important questions remain for future studies. First, what upstream signals activate NFATc1 and promote its binding to CNS-9 in B1a cells? B1a cells can be activated by various stimuli, including Toll-like receptor ligands and cytokines (*26*, *79*, *80*), but how these signals converge to drive NFATc1 activation and subsequent IL-10 production remains unclear. Second, how does NFATc1 cooperate with other transcription factors to regulate IL-10 expression in B cells? While our data identify NFATc1 as a key regulator, cell type–specific and context-dependent IL-10 expression likely involves combinatorial interactions with additional factors. Third, what role does NFATc1-mediated CNS-9 regulation play in other IL-10–dependent processes, such as autoimmunity, cancer, and chronic infection? Further studies using cell type–specific deletion of CNS-9 or NFATc1 in diverse disease models will help address these questions. Finally, what are the genome-wide direct targets and transcriptional programs regulated by NFATc1 in B1a cells? Although our transcriptomic analysis suggests that NFATc1 broadly influences gene expression in B cells beyond *Il10*, integrative approaches combining NFATc1 ChIP-seq with RNA-seq will be required to systematically define direct NFATc1-dependent regulatory networks and to place *Il10* regulation within this broader context.

In conclusion, this study identifies a conserved, enhancer-dependent mechanism by which NFATc1 regulates IL-10 expression in B1a cells, thereby suppressing excessive inflammatory responses during sepsis. These findings enhance our understanding of the molecular regulation

of B cell–derived IL-10 and offer insights for therapeutic strategies targeting the modulation of IL-10 expression in inflammatory disorders.

MATERIALS AND METHODS

Mice

C57BL/6 and congenic *CD45.1*$^{+}$ mice were maintained under specific pathogen–free (SPF) conditions (the Jackson laboratory, USA) in the animal facility of the POSTECH Biotech Center in accordance with institutional ethical guidelines. To minimize genetic variability apart from the target gene, a controlled breeding strategy was implemented. Homozygous WT and CNS-9 KO mice were derived from the same heterozygous parental lineage on a C57BL/6 background and subsequently used for experimental procedures. *NFATc1*$^{fl/fl}$ and *CD19*^{Cre} mice were provided by A. Rao (La Jolla Institute for immunology). For the generation of conditional KO models, *NFATc1*$^{fl/fl}$ mice were crossed with *CD19*^{cre} mice to obtain *CD19*^{cre} *NFATc1*$^{fl/fl}$ conditional KO mice. To establish the combined KO model, CD19^{cre} *NFATc1*$^{fl/fl}$ mice were crossed with CNS-9 KO mice. Heterozygous offspring from this cross were selected and further bred to generate *CD19*^{cre} *NFATc1*$^{fl/fl}$ CNS-9 KO mice. Genotyping was performed using specific primers listed in table S1. Gender- and age-matched mice between 7 and 9 weeks old were used in all experiments. Mice were randomly assigned to experimental groups, with genotype and age balanced across groups. All mice were maintained under SPF conditions in accordance with Institutional Animal Care and Use Committee (IACUC) guidelines from the animal facility of the POSTECH Biotech Center (POSTECH-2021-0029, POSTECH-2022-0011, POSTECH-2022-0011-R1, and POSTECH-2025-0122). Animal experiments were conducted in accordance with the Animal Research: Reporting of In Vivo Experiments (ARRIVE) guidelines. Sample sizes for animal experiments were estimated on the basis of pilot experiments and the "Sample Size Calculations (IACUC)" guidance provided by Boston University (www.bu.edu/research/forms-policies/iacuc-sample-size-calculations; effective 05 March 2024, next review 04 March 2027). Using a power level of 80% and a significance level of $P = 0.01$, we calculated the minimum number of mice required for each in vivo study. To account for potential technical issues during disease induction and progression, one or two additional animals were included per group. No animals were excluded from analysis unless preestablished technical failures occurred.

Generation of CNS-9 KO mice

The CNS-9-targeting plasmid was constructed by cloning the sequences flanking the CNS-9 site into the pOSDupDel vector (MES3974, Open Biosystems), which contains a neomycin resistance (NeoR) gene as a positive selection marker and a thymidine kinase gene as a negative selection marker. To generate CNS-9 KO mice, the CNS-9 fragment was replaced with a NeoR gene cassette flanked by LoxP sites. This construct was electroporated into the 129/Sv J1 embryonic stem (ES) cell line. Properly targeted ES cell clones were selected and subsequently injected into C57BL/6 blastocysts to generate chimeric mice. High-percentage chimeras were bred with C57BL/6 mice to establish germline transmission. The deletion of the CNS-9 allele was confirmed by Southern blot analysis and PCR. Male CNS-9–deficient mice on a 129/Sv × C57BL/6 F1 mixed background were backcrossed with C57BL/6 (B6) females for 10 generations to establish a congenic line. Mice from this congenic line were used for all subsequent experiments.

Single-cell suspension from the spleen, bone marrow, and peritoneal cavity

Single-cell suspensions of splenic lymphocytes were prepared by gently dissociating the spleen through a 100-μm cell strainer. Bone marrow cells were flushed from the femurs using a 26-gauge needle. After centrifugation, the cell pellet was washed with RPMI 1640 supplemented with 10% fetal bovine serum (FBS) (Hyclone). Red blood cells were lysed using ammonium-chloride-potassium (ACK) lysis buffer for 2 min, followed by washing with RPMI 1640 supplemented with additional components. Peritoneal cells were obtained by performing peritoneal lavage with PBS. The collected lavage fluid was centrifuged, and the resulting cell pellet was washed with RPMI 1640 containing 10% FBS before further analysis.

Flow cytometry analysis

For Live/Dead staining, single-cell suspensions from the spleen and peritoneal cavity were stained with Fixable Viability Dye (Invitrogen). For surface marker staining, cells were washed with PBS and stained with the following antibodies: CD45 (30-F11), CD45.1 (A20), CD45.2 (104), CD19 (1D3, 6D5, and SJ25C1), B220 (RA3-6B2), BP-1 (6C3), immunoglobulin D (IgD) (11-26c.2a), IgM (II/41), CD43 (S11), CD43 (1B11), CD5 (53-7.3), CD93 (AA4.1), CD21 (7E9 and eBio8D9), CD23 (B3B4), CD24 (M1/69), GL7 (GL7), CD138 (281-2), CD11b (M1/70), CD11c (N418), F4/80 (BM8), Ly6C (HK1.4), Ly6G (1A8), Gr-1 (RB6-8C5), TER-119 (TER-119), CD3 (17A2), CD3ε (145-2C11), NK1.1 (PK136), TCRγδ (GL3), TCRβ (H57-597), CD4 (RM4-5), CD8a (53-6.7), CD44 (IM7), and CD62L (MEL-14). For intracellular transcription factor staining, cells were fixed using eBioscience/Invitrogen Foxp3 Fix/Perm Buffer, washed with eBioscience/Invitrogen Perm Buffer, and stained with the following antibodies: Foxp3 (FJK-16 s), Bcl-6 (7D1), and Blimp1 (5E7). For intracellular cytokine staining, two stimulation methods were used: (i) Cells were restimulated with PMA (50 ng/ml; Calbiochem) and 2 μM ionomycin in the presence of Golgi-Stop (0.7 μl/ml; BD Biosciences, 554724) and Golgi-Plug (1 μl/ml; BD Biosciences, 555029) for 4 hours. (ii) Cells were restimulated using the Cell Stimulation Cocktail plus protein transport inhibitors (00-4975-03, eBioscience/Invitrogen). After restimulation, cells were washed and stained for surface markers. Cells were then fixed with either eBioscience/Invitrogen Foxp3 Fix/Perm Buffer or eBioscience/Invitrogen Intracellular (IC) Fixation Buffer, washed with Perm Buffer, and stained with the following antibodies: IL-10 (JES5-16E3 and JES3-9D7), IL-6 (MP5-20F3), and IL-1β (NJTEN3). A comprehensive list—including the source, clone, format, and catalog number of all antibodies—is provided in table S2. Cell acquisition was performed using an LSR Fortessa flow cytometer (BD Biosciences) or a CytoFLEX flow cytometer (Beckman Coulter) at the Microbiome Core Facility of POSTECH. Data were analyzed using FlowJo software (Tree Star).

Bioinformatic analysis

Genomic sequences spanning 40 kb of the IL-10 gene were analyzed using web-based alignment tools, including VISTA Browser 2.0 (https://pipeline.lbl.gov/cgi-bin/gateway2) and ECR Browser (https://ecrbrowser.dcode.org/), to identify CNSs. ATAC-seq and RNA-seq data for 10 B cell subsets were obtained from the ImmGen database (www.immgen.org/). OCRs across the *Il10* locus and their corresponding chromatin accessibility scores, as well as IL-10 expression levels, were analyzed using these datasets. Microarray data on transcription factor expression were retrieved from the same

database. Transcription factor binding motifs within CNS-9 were predicted using the rVISTA program (http://rvista.dcode.org), which uses matrices from the TRANSFAC database (TRANSFAC Professional V10.2 library). Publicly available ATAC-seq (GSE103057 and GSE82144), ChIP-seq (GSE82144, GSE33819, GSE92344, GSE32465, and GSE29611), Microarray (GSE21063), and Hi-C data (GSE63525) were retrieved from the National Center for Biotechnology Information Gene Expression Omnibus database. Sequence reads were aligned to the mouse genome (mm10) or human genome (hg19) using Bowtie 2. BedGraph files were generated using HOMER and converted to bigWig format for visualization with the University of California, Santa Cruz bedGraphToBigWig tool. Data visualization was performed using the WashU Epigenome Browser and the Integrative Genomics Viewer.

Cell lines

A20 and Raji B cell lines were obtained from the American Type Culture Collection (MD, USA).

Cloning and mutagenesis of reporter vector

Promoter and CNS regions of the *Il10* locus were amplified from P1 clones by PCR and cloned into the pXPG reporter vector containing the luciferase gene. Primers used for cloning are listed in table S3. To inactivate conserved NFAT binding motifs within the CNS locus, site-directed mutagenesis was performed using the QuickChange Site-Directed Mutagenesis Kit (Stratagene, CA, USA), with primers listed in table S4. To disrupt all predicted NFAT-binding motifs within CNS-9, a fully synthetic mutant CNS-9 fragment was generated by gene synthesis (Bioneer, Korea). All constructs were verified by Sanger sequencing before use in luciferase assays.

Transient transfection and reporter assays

A20 cells were transfected using Lipofectamine 2000 (Invitrogen, CA, USA) or electroporated with the Isoosmolar Electroporation Buffer (Eppendorf, Hamburg, Germany) using a Multiporator system, according to the manufacturer's protocol. Primary B cells were transfected using the Mouse B Cell Nucleofector Kit (Lonza, Cologne, Germany).

For the reporter assay, the pXPG vector was cotransfected into B cells along with the pRL-TK Renilla vector. After 12 hours of transfection, the cells were stimulated with PMA and ionomycin for an additional 24 hours. Reporter activity was then measured using the Dual-Luciferase Assay System (Promega, WI, USA). Firefly luciferase activity was normalized to Renilla luciferase activity.

qRT-PCR analysis

Total RNA was extracted using TRIzol reagent (Molecular Research Center, OH, USA) according to the manufacturer's instructions. cDNA was synthesized from 500 ng of total RNA in a 20 μl of reaction using the ImProm-II Reverse Transcription System (Promega). The qRT-PCR was performed using SYBR Premix Ex Taq (Takara, Shiga, Japan) and a Rotor-Gene Q Real-Time PCR System (QIAGEN), with gene-specific primers listed in table S5. Gene expression was normalized to hypoxanthine-guanine phosphoribosyltransferase for mouse samples and glyceraldehyde-3-phosphate dehydrogenase for human Raji B cells.

ChIP assays

ChIP analysis was performed as previously described, with minor modifications (*81*). Briefly, B cells were stimulated for 1 hour and cross-linked with 2% formaldehyde. After incubation in lysis buffer, cell lysates were sonicated using a Bioruptor (Diagenode, Liège, Belgium) to fragment the DNA. The sheared chromatin was immunoprecipitated using antibodies against NFATc1, NFATc2, or rabbit IgG. DNA-protein complexes were captured using protein G agarose (Millipore) and then reverse cross-linked. The presence of specific DNA sequences was assessed by RT-PCR using primers listed in table S6. As a control, PCR was performed directly on the input DNA, which was purified before immunoprecipitation. ChIP data were normalized to input DNA and presented as relative levels compared to the IgG control.

Electrophoretic mobility shift assay

EMSA was performed as described previously with minor modification (*82*). Double-stranded probes were labeled with γ-32P-ATP (PerkinElmer, MA, USA) by T4 polynucleotide kinase (New England Biolabs, MA, USA) and then purified by G-50 micro column (GE Healthcare, NJ, USA). Nuclear extracts of $CD19^+$ B cells (10 ug) were incubated with 0.1 mg of poly(dI-dC) in standard EMSA binding buffer for 30 min and subsequently mixed with radio-labeled probes for 30 min. Probe sequences were described in table S7. Unlabeled oligomers used as competitors were added to the mixtures 30 min before probe incubation. For supershift assays, nuclear extracts were preincubated with specific antibodies against the target protein. Samples were subjected to 6% nondenaturing polyacrylamide gels in 0.5× tris-borate–EDTA buffer.

3C assay

The 3C assay was performed as previously described (*83*, *84*). B cells were stimulated with PMA and ionomycin for 1 hour and then cross-linked with 2% formaldehyde for 10 minutes. Genomic DNA was digested with the restriction enzyme Xba I for 12 hours and subsequently ligated using T4 DNA ligase. After DNA purification with phenol-chloroform extraction, ligated products were analyzed by RT-PCR. PCR primers for the 3C assay are listed in table S8. As a control, PCR was performed at an intergenic locus of the IL-10 gene using control primers (Con F and Con R), which served as input DNA. Quantitative levels of 3C products were normalized to input DNA.

Mixed bone marrow chimeras

Bone marrow was isolated from the femurs and tibiae of CD45.1 WT mice and CD45.2 CNS-9 KO mice. Mature T cells were depleted using anti-CD4 (BioLegend, 100404) and anti-CD8a microbeads (BioLegend, 100704), and the remaining bone marrow cells were mixed at a 1:1 ratio. CD45.1/CD45.2 recipient mice underwent lethal irradiation (6.5 Gy × 2) and subsequently received a retroorbital injection of 10×10^6 donor bone marrow cells. Chimeric mice were analyzed 8 weeks posttransplantation.

ELISA for IL-6 and IL-10 quantification

Serum concentrations of mouse IL-6 and IL-10, as well as human IL-10 concentrations in culture supernatants, were quantified using commercially available uncoated ELISA kits (Invitrogen) according to the manufacturer's instructions: Mouse IL-6 (catalog no. 88-7064-88), mouse IL-10 (catalog no. 88-7105-88), and Human IL-10 (catalog no. 88-7106-88). A 96-well half-area clear flat-bottom plate (catalog no. 3690, Corning, NY, USA) was coated with capture antibodies provided in each kit and incubated overnight at 4°C. Plates were then washed with ELISA wash buffer (0.05% Tween 20 in PBS) and subsequently blocked with blocking buffer at room temperature for 1 hour. After blocking, appropriately diluted mouse serum

samples (for IL-6 and IL-10) or cell culture supernatants (for human IL-10), together with serially diluted cytokine standards, were added to the wells and incubated overnight at 4°C. Following extensive washing, plates were incubated with biotinylated detection antibodies for 1 hour at room temperature, followed by incubation with streptavidin–horseradish peroxidase for 30 min. After additional washing, 3,3′,5,5′-tetramethylbenzidine (TMB) substrate was added to each well and incubated for 1 to 2 min in a light-protected environment. The enzymatic reaction was stopped by adding 1 N H_2SO_4, and optical density was measured at 450 nm using a TECAN microplate reader. Cytokine concentrations were calculated from standard curves generated using serial dilutions of recombinant IL-6 or IL-10 standards supplied in the respective kits.

LPS-induced sepsis

All experimental mice were sex- and age-matched. For the survival analysis of LPS-induced sepsis, mice were intraperitoneally injected with LPS (30 mg/kg) from *Escherichia coli* O111:B4 (Sigma-Aldrich, L4130), and survival was monitored for 36 hours. For other analyses, mice received an intraperitoneal injection of LPS (5 mg/kg), and experiments were conducted 36 hours later.

Peritoneal B1a cell sorting and adoptive transfer

Peritoneal B1a adoptive transfer experiments were performed as previously described, with minor modifications (*12*). Peritoneal cells were collected by lavage with cold PBS. B1a cells were identified as $PI^-CD19^+B220^{lo/-}CD43^+CD5^+$ cells and sorted using a MoFlo Astrios EQ cell sorter (Beckman Coulter). Post-sort purity was assessed by flow cytometry and was consistently ≥95% for all experiments. Sorted B1a cells were washed twice with sterile PBS and resuspended at 5×10^5 cells in 150 μl of PBS per mouse for adoptive transfer. For adoptive transfer experiments, 5×10^5 $CD45.1^+$ WT B1a cells were injected intraperitoneal into recipient WT or CNS-9 KO mice 1 hour before LPS challenge. Control mice received 150 μl of PBS intraperitoneally as vehicle.

Histology

Lung and liver tissues were collected and fixed in 4% paraformaldehyde solution at 4°C overnight. The tissues were then embedded in paraffin blocks; sectioned at a thickness of 3 μm; deparaffinized; and dehydrated through sequential incubation in xylene, 100% ethanol, and 95% ethanol. The sections were rehydrated in distilled water and stained with hematoxylin (HHS32, Sigma-Aldrich) and eosin (HT110132, Sigma-Aldrich). Images were acquired using a LEICA DFC420 C light microscope. For each lung and liver section, three randomly chosen fields were analyzed to evaluate histopathological changes. Lung tissue damage was evaluated on the basis of four parameters: alveolar congestion, alveolar hemorrhage, infiltration or aggregation of inflammatory cells in the airspace or vessel wall, and thickness of the alveolar wall and hyaline membrane formation. Each parameter was scored on a five-point scale: 0 = normal, 1 = mild damage, 2 = moderate damage, 3 = severe damage, and 4 = maximal damage (*85*). Liver injury was assessed using the Suzuki score, which includes sinusoidal congestion, vacuolization of hepatocyte cytoplasm, and parenchymal necrosis. The sinusoidal congestion and vacuolization of hepatocyte cytoplasm were scored on a five-point scale: 0 = normal, 1 = mild damage, 2 = moderate damage, 3 = severe damage, and 4 = maximal damage. Parenchymal necrosis was scored on the basis of the extent of tissue damage: 0 = no necrosis, 1 = single-cell necrosis, 2 = necrosis affecting up to 30%, 3 = 31 to 60%, and 4 = more than 60% (*86*). All histological evaluations were performed in a blinded manner.

CRISPR mutation of *IL10* CNS-12 in human Raji B cells

PX330 (42230, Addgene) was modified by the addition of a puromycin resistance gene and a green fluorescent protein gene for selection in mammalian cells. sgRNAs were designed using CRISPOR version 5.2 (https://crispor.gi.ucsc.edu/). After annealing the sgRNA oligos, the gRNA duplexes were cloned into the modified PX330 using BbsI (BpiI). sgRNA sequences are listed in the table S9. The vectors were prepared using the Hybrid-Q Plasmid Rapidprep mini. The cloned vectors were isolated using the Hybrid-Q Plasmid Rapidprep Kit (GeneAll, Seoul, Korea). PCR product sequencing was performed by Macrogen (Seoul, Korea). Human Raji B cells were cultured in 10 ml of complete RPMI 1640 medium containing 10% FBS, 5% penicillin/streptomycin, 2 mM L-glutamine, 1 mM sodium pyruvate, nonessential amino acids, and β-mercaptoethanol. The cells were maintained at 37°C in a 5% CO_2 incubator. Raji B cells were electroporated using the Nucleofector 2b Kit V for cell lines (Lonza, VCA-1003) with the GenePulser X cell, following the manufacturer's protocol. Indel frequencies in the CNS-12 region were analyzed using the Synthego ICE tool (https://ice.editco.bio/#/) based on Sanger sequencing data. Primers used for the Sanger sequencing are listed in table S10.

Statistical analysis

Statistical analysis was performed using GraphPad Prism software (v10.4.1, La Jolla, CA, USA). Data are presented as means ± SEM. For single comparisons, statistical significance was determined using a two-tailed unpaired Student's *t* test or a two-tailed paired Student's *t* test, as appropriate. Multiple group comparisons were conducted using one-way analysis of variance (ANOVA) followed by Tukey's post hoc test. For correlation analysis, Pearson's *r* values were calculated, and two-tailed *P* values were assessed. For survival analysis, the log-rank (Mantel-Cox) test was performed. *P* values below 0.05 were considered statistically significant and are reported as follows: $*P < 0.05$, $**P < 0.01$, $***P < 0.001$, and $****P < 0.0001$.

Supplementary Materials

This PDF file includes:

Figs. S1 to S18

Tables S1 to S10

REFERENCES

1. M. Saraiva, P. Vieira, A. O'Garra, Biology and therapeutic potential of interleukin-10. *J. Exp. Med.* **217**, e20190418 (2020).
2. W. Ouyang, A. O'Garra, IL-10 family cytokines IL-10 and IL-22: From basic science to clinical translation. *Immunity* **50**, 871–891 (2019).
3. R. Kuhn, J. Lohler, D. Rennick, K. Rajewsky, W. Muller, Interleukin-10-deficient mice develop chronic enterocolitis. *Cell* **75**, 263–274 (1993).
4. D. J. Berg, R. Kuhn, K. Rajewsky, W. Muller, S. Menon, N. Davidson, G. Grunig, D. Rennick, Interleukin-10 is a central regulator of the response to LPS in murine models of endotoxic shock and the Shwartzman reaction but not endotoxin tolerance. *J. Clin. Invest.* **96**, 2339–2347 (1995).
5. A. O'Garra, P. Vieira, T(H)1 cells control themselves by producing interleukin-10. *Nat. Rev. Immunol.* **7**, 425–428 (2007).
6. R. Madan, F. Demircik, S. Surianarayanan, J. L. Allen, S. Divanovic, A. Trompette, N. Yogev, Y. Gu, M. Khodoun, D. Hildeman, N. Boespflug, M. B. Fogolin, L. Grobe, M. Greweling, F. D. Finkelman, R. Cardin, M. Mohrs, W. Muller, A. Waisman, A. Roers, C. L. Karp, Nonredundant roles for B cell-derived IL-10 in immune counter-regulation. *J. Immunol.* **183**, 2312–2320 (2009).

7. K. Yanaba, J. D. Bouaziz, K. M. Haas, J. C. Poe, M. Fujimoto, T. F. Tedder, A regulatory B cell subset with a unique CD1d^{hi}CD5^{+} phenotype controls T cell-dependent inflammatory responses. *Immunity* **28**, 639–650 (2008).
8. W. van de Veen, B. Stanic, O. F. Wirz, K. Jansen, A. Globinska, M. Akdis, Role of regulatory B cells in immune tolerance to allergens and beyond. *J. Allergy Clin. Immunol.* **138**, 654–665 (2016).
9. E. C. Rosser, C. Mauri, Regulatory B cells: Origin, phenotype, and function. *Immunity* **42**, 607–612 (2015).
10. A. O'Garra, R. Chang, N. Go, R. Hastings, G. Haughton, M. Howard, Ly-1 B (B-1) cells are the main source of B cell-derived interleukin 10. *Eur. J. Immunol.* **22**, 711–717 (1992).
11. K. Miles, J. Simpson, S. Brown, G. Cowan, D. Gray, M. Gray, Immune tolerance to apoptotic self is mediated primarily by regulatory B1a cells. *Front. Immunol.* **8**, 1952 (2017).
12. M. Aziz, N. E. Holodick, T. L. Rothstein, P. Wang, B-1a cells protect mice from sepsis: Critical role of CREB. *J. Immunol.* **199**, 750–760 (2017).
13. R. C. Hardison, Conserved noncoding sequences are reliable guides to regulatory elements. *Trends Genet.* **16**, 369–372 (2000).
14. Y. Zheng, S. Josefowicz, A. Chaudhry, X. P. Peng, K. Forbush, A. Y. Rudensky, Role of conserved non-coding DNA elements in the Foxp3 gene in regulatory T-cell fate. *Nature* **463**, 808–812 (2010).
15. B. Koh, A. Abdul Qayum, R. Srivastava, Y. Fu, B. J. Ulrich, S. C. Janga, M. H. Kaplan, A conserved enhancer regulates Il9 expression in multiple lineages. *Nat. Commun.* **9**, 4803 (2018).
16. D. Chang, Q. Xing, Y. Su, X. Zhao, W. Xu, X. Wang, C. Dong, The conserved non-coding sequences CNS6 and CNS9 control cytokine-induced rorc transcription during T helper 17 cell differentiation. *Immunity* **53**, 614–626.e4 (2020).
17. R. Kawakami, Y. Kitagawa, K. Y. Chen, M. Arai, D. Ohara, Y. Nakamura, K. Yasuda, M. Osaki, N. Mikami, C. A. Lareau, H. Watanabe, G. Kondoh, K. Hirota, N. Ohkura, S. Sakaguchi, Distinct Foxp3 enhancer elements coordinate development, maintenance, and function of regulatory T cells. *Immunity* **54**, 947–961.e8 (2021).
18. S. Dikiy, J. Li, L. Bai, M. Jiang, L. Janke, X. Zong, X. Hao, B. Hoyos, Z. M. Wang, B. Xu, Y. Fan, A. Y. Rudensky, Y. Feng, A distal Foxp3 enhancer enables interleukin-2 dependent thymic Treg cell lineage commitment for robust immune tolerance. *Immunity* **54**, 931–946.e11 (2021).
19. K. Cui, Z. Chen, Y. Cao, S. Liu, G. Ren, G. Hu, D. Fang, D. Wei, C. Liu, J. Zhu, C. Wu, K. Zhao, Restraint of IFN-γ expression through a distal silencer CNS-28 for tissue homeostasis. *Immunity* **56**, 944–958.e6 (2023).
20. M. Saraiva, A. O'Garra, The regulation of IL-10 production by immune cells. *Nat. Rev. Immunol.* **10**, 170–181 (2010).
21. S. Rutz, W. Ouyang, Regulation of interleukin-10 expression. *Adv. Exp. Med. Biol.* **941**, 89–116 (2016).
22. H. Zhang, A. Madi, N. Yosef, N. Chihara, A. Awasthi, C. Pot, C. Lambden, A. Srivastava, P. R. Burkett, J. Nyman, E. Christian, Y. Etminan, A. Lee, H. Stroh, J. Xia, K. Karwacz, P. I. Thakore, N. Acharya, A. Schnell, C. Wang, L. Apetoh, O. Rozenblatt-Rosen, A. C. Anderson, A. Regev, V. K. Kuchroo, An IL-27-driven transcriptional network identifies regulators of IL-10 expression across T helper cell subsets. *Cell Rep.* **33**, 108433 (2020).
23. C. G. Lee, K. H. Kang, J. S. So, H. K. Kwon, J. S. Son, M. K. Song, A. Sahoo, H. J. Yi, K. C. Hwang, T. Matsuyama, K. Yui, S. H. Im, A distal cis-regulatory element, CNS-9, controls NFAT1 and IRF4-mediated IL-10 gene activation in T helper cells. *Mol. Immunol.* **46**, 613–621 (2009).
24. M. Saraiva, J. R. Christensen, A. V. Tsytsykova, A. E. Goldfeld, S. C. Ley, D. Kioussis, A. O'Garra, Identification of a macrophage-specific chromatin signature in the IL-10 locus. *J. Immunol.* **175**, 1041–1046 (2005).
25. R. C. Hsueh, R. H. Scheuermann, Tyrosine kinase activation in the decision between growth, differentiation, and death responses initiated from the B cell antigen receptor. *Adv. Immunol.* **75**, 283–316 (2000).
26. P. Antony, J. B. Petro, G. Carlesso, N. P. Shinners, J. Lowe, W. N. Khan, B cell receptor directs the activation of NFAT and NF-κB via distinct molecular mechanisms. *Exp. Cell Res.* **291**, 11–24 (2003).
27. M. Marklin, J. S. Heitmann, J. Kauer, S. Wirths, M. R. Muller, Genetic loss of NFAT2 (NFATc1) impairs B cell development of B1 and B2 B cells. *Cell. Immunol.* **349**, 104048 (2020).
28. A. Rao, C. Luo, P. G. Hogan, Transcription factors of the NFAT family: Regulation and function. *Annu. Rev. Immunol.* **15**, 707–747 (1997).
29. P. G. Hogan, L. Chen, J. Nardone, A. Rao, Transcriptional regulation by calcium, calcineurin, and NFAT. *Genes Dev.* **17**, 2205–2232 (2003).
30. W. M. Flanagan, B. Corthesy, R. J. Bram, G. R. Crabtree, Nuclear association of a T-cell transcription factor blocked by FK-506 and cyclosporin A. *Nature* **352**, 803–807 (1991).
31. H. Yoshida, C. A. Lareau, R. N. Ramirez, S. A. Rose, B. Maier, A. Wroblewska, F. Desland, A. Chudnovskiy, A. Mortha, C. Dominguez, J. Tellier, E. Kim, D. Dwyer, S. Shinton, T. Nabekura, Y. Qi, B. Yu, M. Robinette, K. W. Kim, A. Wagers, A. Rhoads, S. L. Nutt, B. D. Brown, S. Mostafavi, J. D. Buenrostro, C. Benoist, Immunological Genome Project, The cis-regulatory atlas of the mouse immune system. *Cell* **176**, 897–912.e20 (2019).
32. M. Mandal, M. Maienschein-Cline, P. Maffucci, M. Veselits, D. E. Kennedy, K. C. McLean, M. K. Okoreeh, S. Karki, C. Cunningham-Rundles, M. R. Clark, BRWD1 orchestrates epigenetic landscape of late B lymphopoiesis. *Nat. Commun.* **9**, 3888 (2018).
33. K. R. Kieffer-Kwon, K. Nimura, S. S. P. Rao, J. Xu, S. Jung, A. Pekowska, M. Dose, E. Stevens, E. Mathe, P. Dong, S. C. Huang, M. A. Ricci, L. Baranello, Y. Zheng, F. Tomassoni Ardori, W. Resch, D. Stavreva, S. Nelson, M. McAndrew, A. Casellas, E. Finn, C. Gregory, B. G. St Hilaire, S. M. Johnson, W. Dubois, M. P. Cosma, E. Batchelor, D. Levens, R. D. Phair, T. Misteli, L. Tessarollo, G. Hager, M. Lakadamyali, Z. Liu, M. Floer, H. Shroff, E. L. Aiden, R. Casellas, Myc regulates chromatin decompaction and nuclear architecture during B cell activation. *Mol. Cell* **67**, 566–578.e10 (2017).
34. A. Yamane, W. Resch, N. Kuo, S. Kuchen, Z. Li, H. W. Sun, D. F. Robbiani, K. McBride, M. C. Nussenzweig, R. Casellas, Deep-sequencing identification of the genomic targets of the cytidine deaminase AID and its cofactor RPA in B lymphocytes. *Nat. Immunol.* **12**, 62–69 (2011).
35. S. J. Horton, G. Giotopoulos, H. Yun, S. Vohra, O. Sheppard, R. Bashford-Rogers, M. Rashid, A. Clipson, W. I. Chan, D. Sasca, L. Yiangou, H. Osaki, F. Basheer, P. Gallipoli, N. Burrows, A. Erdem, A. Sybirna, S. Foerster, W. Zhao, T. Sustic, A. Petrunkina Harrison, E. Laurenti, J. Okosun, D. Hodson, P. Wright, K. G. Smith, P. Maxwell, J. Fitzgibbon, M. Q. Du, D. J. Adams, B. J. P. Huntly, Early loss of Crebbp confers malignant stem cell properties on lymphoid progenitors. *Nat. Cell Biol.* **19**, 1093–1104 (2017).
36. S. Bhattacharyya, J. Deb, A. K. Patra, D. A. Thuy Pham, W. Chen, M. Vaeth, F. Berberich-Siebelt, S. Klein-Hessling, E. D. Lamperti, K. Reifenberg, J. Jellusova, A. Schweizer, L. Nitschke, E. Leich, A. Rosenwald, C. Brunner, S. Engelmann, U. Bommhardt, A. Avots, M. R. Muller, E. Kondo, E. Serfling, NFATc1 affects mouse splenic B cell function by controlling the calcineurin–NFAT signaling network. *J. Exp. Med.* **208**, 823–839 (2011).
37. M. D. Thomas, C. S. Kremer, K. S. Ravichandran, K. Rajewsky, T. P. Bender, c-Myb is critical for B cell development and maintenance of follicular B cells. *Immunity* **23**, 275–286 (2005).
38. B. Sun, S. Mallampati, Y. Gong, D. Wang, V. Lefebvre, X. Sun, Sox4 is required for the survival of pro-B cells. *J. Immunol.* **190**, 2080–2089 (2013).
39. Y. Sugiyama, M. Fujiwara, A. Sakamoto, H. Tsushima, A. Nishikimi, M. Maruyama, The immunosenescence-related factor DOCK11 is involved in secondary immune responses of B cells. *Immun. Ageing* **19**, 2 (2022).
40. E. M. Schaeffer, P. L. Schwartzberg, Tec family kinases in lymphocyte signaling and function. *Curr. Opin. Immunol.* **12**, 282–288 (2000).
41. J. Klein, W. Ju, J. Heyer, B. Wittek, T. Haneke, P. Knaus, R. Kucherlapati, E. P. Bottinger, L. Nitschke, B. Kneitz, B cell-specific deficiency for Smad2 in vivo leads to defects in TGF-beta-directed IgA switching and changes in B cell fate. *J. Immunol.* **176**, 2389–2396 (2006).
42. I. Y. Hwang, K. S. Hwang, C. Park, K. A. Harrison, J. H. Kehrl, Rgs13 constrains early B cell responses and limits germinal center sizes. *PLOS ONE* **8**, e60139 (2013).
43. B. Guo, T. L. Rothstein, RasGRP1 is an essential signaling molecule for development of B1a cells with autoantigen receptors. *J. Immunol.* **196**, 2583–2590 (2016).
44. M. Garis, L. A. Garrett-Sinha, Notch signaling in B cell immune responses. *Front. Immunol.* **11**, 609324 (2020).
45. D. T. Avery, A. Kane, T. Nguyen, A. Lau, A. Nguyen, H. Lenthall, K. Payne, W. Shi, H. Brigden, E. French, J. Bier, J. R. Hermes, D. Zahra, W. A. Sewell, D. Butt, M. Elliott, K. Boztug, I. Meyts, S. Choo, P. Hsu, M. Wong, L. J. Berglund, P. Gray, M. O'Sullivan, T. Cole, S. M. Holland, C. S. Ma, C. Burkhart, L. M. Corcoran, T. G. Phan, R. Brink, G. Uzel, E. K. Deenick, S. G. Tangye, Germline-activating mutations in PIK3CD compromise B cell development and function. *J. Exp. Med.* **215**, 2073–2095 (2018).
46. G. Tumurkhuu, N. Koide, J. Dagvadorj, A. S. Noman, Y. Khuda Il, T. Naiki, T. Komatsu, T. Y. Yoshida, B1 cells produce nitric oxide in response to a series of toll-like receptor ligands. *Cell. Immunol.* **261**, 122–127 (2010).
47. S. Takatsuka, H. Yamada, K. Haniuda, H. Saruwatari, M. Ichihashi, J. C. Renauld, D. Kitamura, IL-9 receptor signaling in memory B cells regulates humoral recall responses. *Nat. Immunol.* **19**, 1025–1034 (2018).
48. X. Wang, G. Wang, Z. Wang, B. Liu, N. Han, J. Li, C. Lu, X. Liu, Q. Zhang, Q. Yang, G. Wang, PD-1-expressing B cells suppress CD4^{+} and CD8^{+} T cells via PD-1/PD-L1-dependent pathway. *Mol. Immunol.* **109**, 20–26 (2019).
49. Y. Yang, X. Li, Z. Ma, C. Wang, Q. Yang, M. Byrne-Steele, R. Hong, Q. Min, G. Zhou, Y. Cheng, G. Qin, J. V. Youngyunpipatkul, J. B. Wing, S. Sakaguchi, C. Toonstra, L. X. Wang, J. G. Vilches-Moure, D. Wang, M. P. Snyder, J. Y. Wang, J. Han, L. A. Herzenberg, CTLA-4 expression by B-1a B cells is essential for immune tolerance. *Nat. Commun.* **12**, 525 (2021).
50. S. Mostafavi, H. Yoshida, D. Moodley, H. LeBoite, K. Rothamel, T. Raj, C. J. Ye, N. Chevrier, S. Y. Zhang, T. Feng, M. Lee, J. L. Casanova, J. D. Clark, M. Hegen, J. B. Telliez, N. Hacohen, P. L. De Jager, A. Regev, D. Mathis, C. Benoist, C., Immunological Genome Project Consortium, Parsing the interferon transcriptional network and its disease associations. *Cell* **164**, 564–578 (2016).

51. K. Tedford, M. Steiner, S. Koshutin, K. Richter, L. Tech, Y. Eggers, I. Jansing, K. Schilling, A. E. Hauser, M. Korthals, K. D. Fischer, The opposing forces of shear flow and sphingosine-1-phosphate control marginal zone B cell shuttling. *Nat. Commun.* **8**, 2261 (2017).
52. V. Muir, S. Sagadiev, S. Liu, U. Holder, A. M. Armendariz, E. Suchland, I. Meitlis, N. Camp, N. Giltiay, J. M. Tam, E. C. Garner, C. N. Wivagg, D. Shows, R. G. James, A. Lacy-Hulbert, M. Acharya, Transcriptomic analysis of pathways associated with ITGAV/alpha(v) integrin-dependent autophagy in human B cells. *Autophagy* **19**, 926–942 (2023).
53. J. A. Green, K. Suzuki, B. Cho, L. D. Willison, D. Palmer, C. D. Allen, T. H. Schmidt, Y. Xu, R. L. Proia, S. R. Coughlin, J. G. Cyster, The sphingosine 1-phosphate receptor S1P(2) maintains the homeostasis of germinal center B cells and promotes niche confinement. *Nat. Immunol.* **12**, 672–680 (2011).
54. C. Cobaleda, A. Schebesta, A. Delogu, M. Busslinger, Pax5: The guardian of B cell identity and function. *Nat. Immunol.* **8**, 463–470 (2007).
55. A. Barinov, L. Luo, P. Gasse, V. Meas-Yedid, E. Donnadieu, F. Arenzana-Seisdedos, P. Vieira, Essential role of immobilized chemokine CXCL12 in the regulation of the humoral immune response. *Proc. Natl. Acad. Sci. U.S.A.* **114**, 2319–2324 (2017).
56. M. Al-Alwan, S. Hou, T. T. Zhang, K. Makondo, A. J. Marshall, Bam32/DAPP1 promotes B cell adhesion and formation of polarized conjugates with T cells. *J. Immunol.* **184**, 6961–6969 (2010).
57. S. Kadauke, G. A. Blobel, Chromatin loops in gene regulation. *Biochim. Biophys. Acta* **1789**, 17–25 (2009).
58. A. Smallwood, B. Ren, Genome organization and long-range regulation of gene expression by enhancers. *Curr. Opin. Cell Biol.* **25**, 387–394 (2013).
59. M. C. Pils, F. Pisano, N. Fasnacht, J. M. Heinrich, L. Groebe, A. Schippers, B. Rozell, R. S. Jack, W. Muller, Monocytes/macrophages and/or neutrophils are the target of IL-10 in the LPS endotoxemia model. *Eur. J. Immunol.* **40**, 443–448 (2010).
60. ENCODE Project Consortium, An integrated encyclopedia of DNA elements in the human genome. *Nature* **489**, 57–74 (2012).
61. S. S. Rao, M. H. Huntley, N. C. Durand, E. K. Stamenova, I. D. Bochkov, J. T. Robinson, A. L. Sanborn, I. Machol, A. D. Omer, E. S. Lander, E. L. Aiden, A 3D map of the human genome at kilobase resolution reveals principles of chromatin looping. *Cell* **159**, 1665–1680 (2014).
62. V. Gotea, A. Visel, J. M. Westlund, M. A. Nobrega, L. A. Pennacchio, I. Ovcharenko, Homotypic clusters of transcription factor binding sites are a key component of human promoters and enhancers. *Genome Res.* **20**, 565–577 (2010).
63. S. Rao, K. Ahmad, S. Ramachandran, Cooperative binding between distant transcription factors is a hallmark of active enhancers. *Mol. Cell* **81**, 1651–1665.e4 (2021).
64. T. T. Yang, C. W. Chow, Transcription cooperation by NFAT.C/EBP composite enhancer complex. *J. Biol. Chem.* **278**, 15874–15885 (2003).
65. B. Stoermann, K. Kretschmer, S. Duber, S. Weiss, B-1a cells are imprinted by the microenvironment in spleen and peritoneum. *Eur. J. Immunol.* **37**, 1613–1620 (2007).
66. M. Aziz, Y. Ode, M. Zhou, M. Ochani, N. E. Holodick, T. L. Rothstein, P. Wang, B-1a cells protect mice from sepsis-induced acute lung injury. *Mol. Med.* **24**, 26 (2018).
67. K. Itoh, S. Hirohata, The role of IL-10 in human B cell activation, proliferation, and differentiation. *J. Immunol.* **154**, 4341–4350 (1995).
68. H. S. Kim, J. H. Lee, H. D. Han, A. R. Kim, S. T. Nam, H. W. Kim, Y. H. Park, D. Lee, M. B. Lee, Y. M. Park, H. S. Kim, Y. M. Kim, J. C. You, W. S. Choi, Autocrine stimulation of IL-10 is critical to the enrichment of IL-10-producing $CD40^{hi}CD5^{+}$ regulatory B cells in vitro and in vivo. *BMB Rep.* **48**, 54–59 (2015).
69. Y. Levy, J. C. Brouet, Interleukin-10 prevents spontaneous death of germinal center B cells by induction of the bcl-2 protein. *J. Clin. Invest.* **93**, 424–428 (1994).
70. C. Mauri, P. A. Blair, Regulatory B cells in autoimmunity: Developments and controversies. *Nat. Rev. Rheumatol.* **6**, 636–643 (2010).
71. S. E. McGettigan, G. F. Debes, Immunoregulation by antibody secreting cells in inflammation, infection, and cancer. *Immunol. Rev.* **303**, 103–118 (2021).
72. F. Rousset, E. Garcia, T. Defrance, C. Peronne, N. Vezzio, D. H. Hsu, R. Kastelein, K. W. Moore, J. Banchereau, Interleukin 10 is a potent growth and differentiation factor for activated human B lymphocytes. *Proc. Natl. Acad. Sci. U.S.A.* **89**, 1890–1893 (1992).
73. D. Polychronopoulos, J. W. D. King, A. J. Nash, G. Tan, B. Lenhard, Conserved non-coding elements: Developmental gene regulation meets genome organization. *Nucleic Acids Res.* **45**, 12611–12624 (2017).
74. E. Cano-Gamez, G. Trynka, From GWAS to function: Using functional genomics to identify the mechanisms underlying complex diseases. *Front. Genet.* **11**, 424 (2020).
75. C. T. Stankey, C. Bourges, L. M. Haag, T. Turner-Stokes, A. P. Piedade, C. Palmer-Jones, I. Papa, M. Silva Dos Santos, Q. Zhang, A. J. Cameron, A. Legrini, T. Zhang, C. S. Wood, F. N. New, L. O. Randzavola, L. Speidel, A. C. Brown, A. Hall, F. Saffioti, E. C. Parkes, W. Edwards, H. Direskeneli, P. C. Grayson, L. Jiang, P. A. Merkel, G. Saruhan-Direskeneli, A. H. Sawalha, E. Tombetti, A. Quaglia, D. Thorburn, J. C. Knight, A. P. Rochford, C. D. Murray, P. Divakar, M. Green, E. Nye, J. I. MacRae, N. B. Jamieson, P. Skoglund, M. Z. Cader, C. Wallace, D. C. Thomas, J. C. Lee, A disease-associated gene desert directs macrophage inflammation through ETS2. *Nature* **630**, 447–456 (2024).
76. J. Z. Liu, S. van Sommeren, H. Huang, S. C. Ng, R. Alberts, A. Takahashi, S. Ripke, J. C. Lee, L. Jostins, T. Shah, S. Abedian, J. H. Cheon, J. Cho, N. E. Dayani, L. Franke, Y. Fuyuno, A. Hart, R. C. Juyal, G. Juyal, W. H. Kim, A. P. Morris, H. Poustchi, W. G. Newman, V. Midha, T. R. Orchard, H. Vahedi, A. Sood, J. Y. Sung, R. Malekzadeh, H. J. Westra, K. Yamazaki, S. K. Yang, International Multiple Sclerosis Genetics Consortium, International IBD Genetics Consortium, J. C. Barrett, B. Z. Alizadeh, M. Parkes, T. Bk, M. J. Daly, M. Kubo, C. A. Anderson, R. K. Weersma, Association analyses identify 38 susceptibility loci for inflammatory bowel disease and highlight shared genetic risk across populations. *Nat. Genet.* **47**, 979–986 (2015).
77. J. Bentham, D. L. Morris, D. S. C. Graham, C. L. Pinder, P. Tombleson, T. W. Behrens, J. Martin, B. P. Fairfax, J. C. Knight, L. Chen, J. Replogle, A. C. Syvanen, L. Ronnblom, R. R. Graham, J. E. Wither, J. D. Rioux, M. E. Alarcon-Riquelme, T. J. Vyse, Genetic association analyses implicate aberrant regulation of innate and adaptive immunity genes in the pathogenesis of systemic lupus erythematosus. *Nat. Genet.* **47**, 1457–1464 (2015).
78. K. Kweon, E. S. Shin, K. J. Park, J. K. Lee, Y. Joo, H. W. Kim, Genome-wide analysis reveals four novel loci for attention-deficit hyperactivity disorder in Korean youths. *Soa Chongsonyon Chongsin Uihak* **29**, 62–72 (2018).
79. R. Berland, H. H. Wortis, Normal B-1a cell development requires B cell-intrinsic NFATc1 activity. *Proc. Natl. Acad. Sci. U.S.A.* **100**, 13459–13464 (2003).
80. L. Genestier, M. Taillardet, P. Mondiere, H. Gheit, C. Bella, T. Defrance, TLR agonists selectively promote terminal plasma cell differentiation of B cell subsets specialized in thymus-independent responses. *J. Immunol.* **178**, 7779–7786 (2007).
81. J. D. Nelson, O. Denisenko, K. Bomsztyk, Protocol for the fast chromatin immunoprecipitation (ChIP) method. *Nat. Protoc.* **1**, 179–185 (2006).
82. L. M. Hellman, M. G. Fried, Electrophoretic mobility shift assay (EMSA) for detecting protein-nucleic acid interactions. *Nat. Protoc.* **2**, 1849–1861 (2007).
83. J. Dekker, The three 'C' s of chromosome conformation capture: Controls, controls, controls. *Nat. Methods* **3**, 17–21 (2006).
84. H. Hagege, P. Klous, C. Braem, E. Splinter, J. Dekker, G. Cathala, W. de Laat, T. Forne, Quantitative analysis of chromosome conformation capture assays (3C-qPCR). *Nat. Protoc.* **2**, 1722–1733 (2007).
85. D. Wang, Y. Li, H. Yang, X. Shen, X. Shi, C. Li, Y. Zhang, X. Liu, B. Jiang, X. Zhu, H. Zhang, X. Li, H. Bai, Q. Yang, W. Gao, F. Bai, Y. Ji, Q. Chen, J. Ben, Disruption of TIGAR-TAK1 alleviates immunopathology in a murine model of sepsis. *Nat. Commun.* **15**, 4340 (2024).
86. S. Suzuki, L. H. Toledo-Pereyra, F. J. Rodriguez, D. Cejalvo, Neutrophil infiltration as an important factor in liver ischemia and reperfusion injury. Modulating effects of FK506 and cyclosporine. *Transplantation* **55**, 1265–1272 (1993).

Acknowledgments: We thank K. S. Lee for mouse husbandry. **Funding:** This work was supported by grants from the National Research Foundation of Korea (NRF), funded by the Ministry of Science and ICT (MSIT) (RS-2023-00260454 and RS-2024-00345575 to S.-H.I., Basic Science Research Institute Fund (RS-2021-NR060139 to S.-H.I.), NRF-2019H1A2A1077180 to S.W.K., and NRF-2021R1A2C1010771 to J.-S.S.). Basic Science Research Institute Fund (NRF grant RS-2021-NR060139 to S.-H.I.). **Author contributions:** Conceptualization: S.W.K., J.-S.S., and S.-H.I. Methodology: S.W.K., J.-S.S., and S.-H.I. Investigation: S.W.K., J.-S.S., J.N., H.E.P., K.H.S., W.H., C.J.K., and S.-H.I. Validation: S.W.K., J.N., H.E.P., J.-S.S., and S.-H.I. Formal analysis: S.W.K., J.-S.S., and S.-H.I. Data curation: S.W.K. and G.-C.K. Software: S.W.K. and G.-C.K. Visualization: S.W.K. and S.-H.I. Resources: S.-H.I. Writing—original draft: S.W.K. and J.-S.S. Writing—review and editing: S.W.K., J.-S.S., and S.-H.I. Supervision: J.-S.S. and S.-H.I. Project administration: S.-H.I. Funding acquisition: J.-S.S. and S.-H.I. **Competing interests:** S.-H.I. is the CEO and major shareholder of ImmunoBiome but declares no conflicts of interest for this paper. Other authors declare that they have no competing interests. **Data, code, and materials availability:** All data needed to evaluate and reproduce the results in the paper are present in the paper and/or the Supplementary Materials. This study did not generate new materials.

Submitted 10 October 2025
Accepted 20 March 2026
Published 24 April 2026
10.1126/sciadv.aec7779

ScienceAdvances

Conserved noncoding sequence-9 regulates NFATc1-mediated IL-10 expression in B cells to control inflammatory responses

Seung Won Kim, Jaegyun Noh, Hye Eun Park, Ki Hurn So, Won Hwang, Gi-Chen Kim, Chan Johng Kim, Jae-Seon So, and Sin-Hyeog Im

Sci. Adv. **12** (17), eaec7779. DOI: 10.1126/sciadv.aec7779

Science Advances (ISSN 2375-2548) is published by the American Association for the Advancement of Science. 1200 New York Avenue NW, Washington, DC 20005. The title *Science Advances* is a registered trademark of AAAS.